THE UNIVERSITY OF CALGARY

Pressure Fluctuations in Agglomerating Gas-Fluidized Beds

by

Jing Li

A THESIS

SUBMITTED TO THE FACULTY OF GRADUATE STUDIES

IN PARTIAL FULFILLMENT OF THE REQUIREMENTS FOR THE

DEGREE OF MASTER OF SCIENCE IN CHEMICAL ENGINEERING

DEPARTMENT OF CHEMICAL AND PETROLEUM ENGINEERING

CALGARY, ALBERTA

May, 2000

Abstract

Many industrial gas-fluidized beds are operated under conditions in which the bed material tends to agglomerate due to the cohesive nature of the particles comprising the bed. This cohesiveness may be an inherent property of the bed particles at some temperature, or may be due to the addition of a liquid to the bed forming a sticky coating on the particles.

In many gas-fluidized processes, the particulate bed material is contacted with a liquid feed stream. If the liquid feed rate is sufficiently high, the liquid coated particles may stick together resulting in process upset due to bed agglomeration and defluidization, a condition commonly known in industry as "bogging". Bogging is an important concern in the operation of fluid coking units for upgrading oil sands bitumen. The consequences of bogging can be severe, possibly requiring complete unit shut-down and clean-out. It is therefore imperative that the onset of bogging be detected and eliminated in order to prevent unit upset and shut-down.

A fundamental experimental study was undertaken in order to investigate the bogging phenomena and to find an effective method of detecting the onset of bogging prior to a complete loss of fluidization. Experiments were carried out in an air fluidized bed.

Different sizes of Geldart group A and B materials were studied. The effect of bed agglomeration and bogging on fluctuations in the bed pressure were measured.

The bed pressure data were analyzed using several common signal analysis techniques including the standard deviation function, the power spectral density function and the autocovariance function. Of these techniques, the standard deviation function was found to be the best method for detecting the onset of bogging. The results of this work may be applied to the development of a process sensor for detecting bogging in industrial scale units.

Acknowledgements

I would like to express my sincere gratitude to my supervisor, Dr. Bruce J. Milne for his continuous enthusiasm, patience and encouragement. His ongoing support and guidance is responsible for much of this work.

I would also like to thank Dr. Caroline Hyndman and Dr. Ronald Hugo for reviewing this thesis. Dr. Hyndman gave me some good suggestions during my experiments. Her help is gratefully acknowledged.

My thanks also to Mike Grigg for his continual technical support, Derek Verhegge for building my fluidized bed, Mark Hancock for his great help on the rotameter calibration and Jake Neudorf for lending me the needle valve.

I would like to acknowledge Rajesh Kumar Jakher and Ian Wright for their friendly help when I had questions. Also thanks to all friends and fellow graduate students who made my stay here lively and cheerful.

The financial support of the Natural Sciences and Engineering Research Council of Canada is gratefully acknowledged.

Finally, I must thank my family. Their endless love and support provide me a feeling of strength. This thesis is dedicated to them.

Table of Contents

List of Tables

List of Figures

Nomenclature

A	cross section area of a fluidized bed, m^2
a, b	empirical coefficient in Equation 2.1
C_{xx}	auto-covariance function
C_{xy}	cross-covariance function
d_{bo}	bubble diameter just above the distributor, m
d_b	bubble diameter, m
d_{pi}	particle diameter in size interval i, m
d_p	particle diameter based on screen analysis, m
d_t	bed diameter, m
F	pressure increase due to water injection, N
G	water weight injected into the bed, N
j	imaginary number
P	pressure, N/m^2
R_{xx}	auto-correlation function
R_{xy}	cross-correlation function
$S_{xx}(f)$	autospectral density function or power spectral density function
$S_{xy}(f)$	cross-spectral density function
T	period of sampling, s
T_s	minimum sintering temperature, K
u_o	superficial gas velocity, m/s

u_b	bubble rise velocity, m/s
u_{br}	bubble rise velocity with respect to the emulsion phase, m/s
u_{mf}	minimum fluidization velocity, m/s
u_t	terminal settling velocity, m/s
x_i	weight fraction of material in size interval i
x(t), y(t)	random variables

Greek Letters

ρ_s, ρ_g	density of solids and air, kg/m^3
ε_{mf}	void fraction at minimum fluidizing condition, dimensionless
μ	mean value
μ_g	air viscosity, kg/m s
ϕ_s	sphericity of particles, dimensionless
φ^2	mean square value
σ^2	variance
τ	time shift variable

Abbreviations

PSD	power spectral density function

CHAPTER 1

Introduction

1.1 Introduction

Fluidization is an operation involving a bed of particulate solids suspended in a fluid media in which the net drag force caused by the flow of the fluid balances the effective weight of the particles. Fluidization technology dates back over 100 years to the fluidized calcining furnace in 1879 (Pugsley, 1995). However, the first large scale and commercially significant application is generally recognized as being the Winkler coal gasifier (Winkler, 1922). Fluidization as a unit operation has achieved widespread and long lasting success in physical, chemical, petrochemical and biochemical processing. Fluidization systems provide high macromixing, yielding large axial dispersion of phases and high reactant conversion for reaction kinetics favoring completely mixed flow patterns.

Many industrial fluidized beds are operated under conditions in which the bed material tends to agglomerate due to the stickiness of the bed material. This stickiness may be an inherent property of the particles at some temperatures, or may occur if a liquid is deposited upon the bed material. The formation of particle aggregates due to agglomeration can result in uneven, partial or even a total loss of fluidization. Defluidization may occur even though the bed is operated at gas velocities much higher

than the minimum fluidization conditions of the initial bed material. Therefore, determination of minimum fluidization conditions based on the initial feed particles in an agglomerating fluidized bed is not very meaningful. Other limiting conditions on the fluidization velocity such as the bed temperature or the amount of liquid added to the bed can have a critical effect on the operation of the unit.

1.2 Background

In many gas-fluidized processes, the particulate bed material is contacted with a liquid feed stream. If the liquid feed rate is sufficiently high, the liquid coated particles may stick together resulting in process upset due to bed agglomeration and defluidization, a condition commonly known in industry as "bogging". For example, bogging is an important concern in the operation of fluid coking units for upgrading heavy petroleum feedstocks such as oil sands bitumen.

Fluid coking is a continuous fluid bed process for upgrading residual petroleum stocks to gas oil, naphtha, gas and coke. The first commercial fluid coker went on-stream in late 1954 (Busch, 1970). Figure 1.1 is a schematic flow plan of a fluid coker. Fluid coking uses two major vessels; a reactor and a burner. The residuum feed is injected into the reactor where it is thermally cracked to vaporized products and coke which is deposited on fluid coke particles. Fluid coke circulates between the vessels to provide heat to the

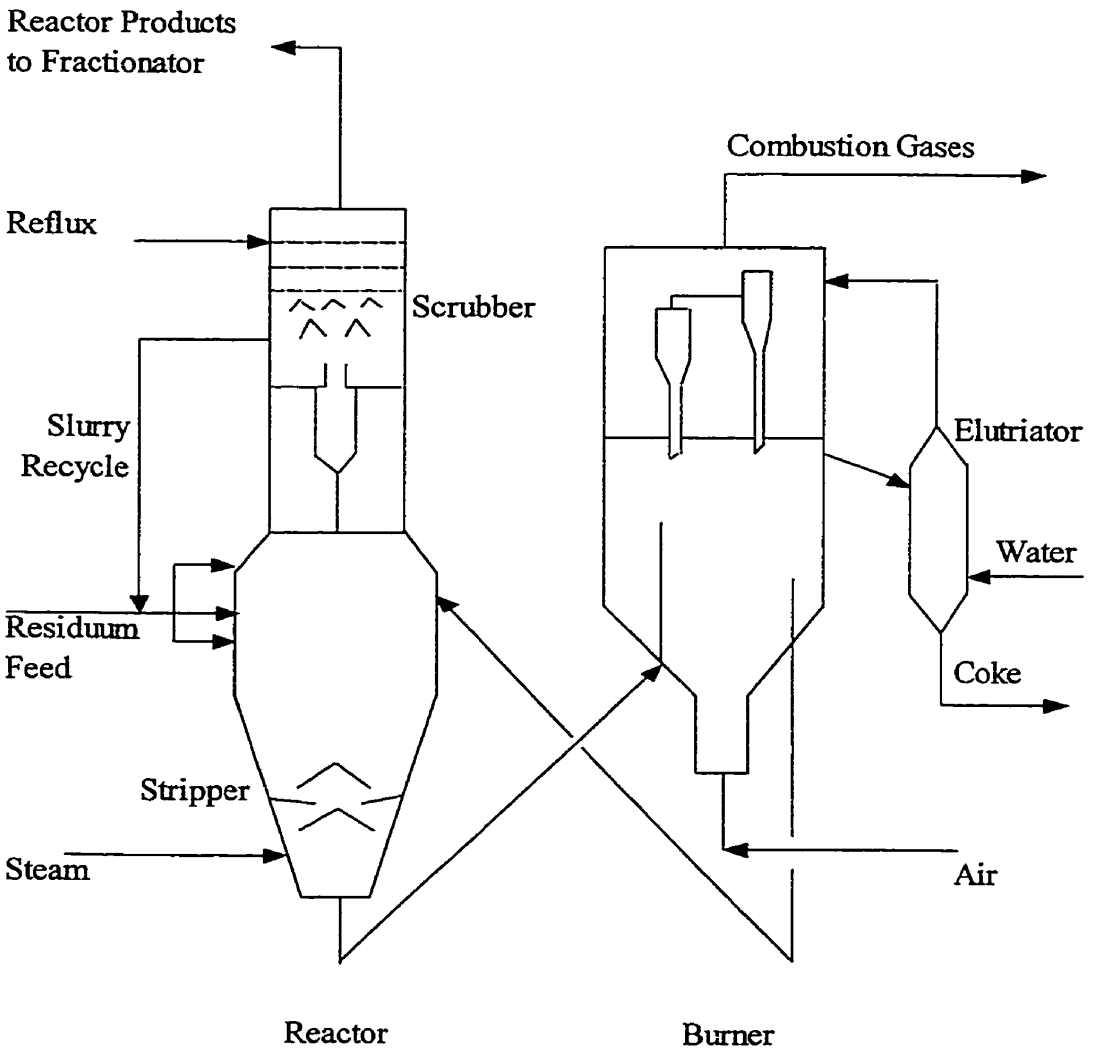

Figure 1.1 Schematic Flow Plan of a Fluid Coker

reactor. Steam is introduced into the bottom of the reactor to fluidize the coke particles and to strip residual hydrocarbon vapor from the coke.

Vapor products leave the reactor bed and pass through cyclones which remove most of the entrained coke. The cyclones discharge the vapor into a scrubber in which the remaining coke dust is removed and the products are cooled to condense the heavy tar. The resulting slurry is recycled to the reactor. The scrubber overhead vapors are then sent to a fractionator where they are separated into wet gas, naphtha, and various gas oil fractions. The wet gas is compressed and further fractionated into the desired components.

In the reactor the coke particles flow down through the vessel into the stripping zone. The stripped coke then flows down a standpipe and through a slide valve which controls the reactor bed level. A riser carries the cold coke to the burner. Air is introduced to the burner to burn part of the coke to provide heat for the reactor. The hot coke from the burner flows down a standpipe through a slide valve which controls coke flow and thus the reactor bed temperature. A riser carries the hot coke to the top of the reactor bed. Combustion products from the burner bed pass through two stages of cyclones to recover coke fines and return them to the burner.

Coke is withdrawn from the burner to keep the solids inventory constant. To keep the coke from becoming too coarse, large particles are selectively removed in a quench

elutriator drum and coke fines are returned to the burner. The product coke is quenched with water in the quench elutriator drum and pneumatically transported to storage. The typical properties of fluid coke are shown in Table 1.1.

Table 1.1 Typical Fluid Coke Properties (Kett *et al.*, 1974)

	Bulk density kg/m^3	Particle density kg/m^3	Average particle size μm	Surface area m^2/g
Fluid coke	950	1500	170-240	<12

Economics dictate that the feed rate of bitumen to the fluid coker be as high as possible without causing the bed to bog. If the feed injection rate exceeds the vaporization rate for an extended period of time, the thickness of the tacky oil film on the particles will increase until the particles rapidly agglomerate, causing the bed to lose fluidity. When fluidization is lost, the heat transfer rate is greatly reduced, further aggravating the condition, and coke circulation cannot be maintained.

Bogging is also a concern in a number of metallurgical and polymerization processes in which fluidized beds of solid particles are operated at temperatures very close to the melting point. The consequences of bogging can be severe, possibly requiring complete unit shut-down and clean-out. It is therefore imperative that the onset of bogging be detected and eliminated in order to prevent unit upset and shut-down.

1.3 Objective

In spite of the fact that the existence of the bogging phenomena has been known since the invention of the fluid coker, a complete understanding of the behaviour of agglomerating particles in fluidized beds is lacking. Previous studies of agglomerative fluidization which mention methods to detect bogging are few.

The main objective of this work is to conduct a fundamental investigation of the bogging phenomena and to develop a method for detecting the onset of bogging in fluid coking units and other large scale fluidized beds which can be implemented in a process control scheme to prevent unit upset and shut-down.

The following chapter will provide an overview of previous studies of particle agglomeration, including agglomeration due to high temperature and liquid deposition. The effect of agglomeration on pressure fluctuations in a fluidized bed and the methods used to analyze pressure fluctuations will also be presented in this chapter. Chapter 3 will discuss the experimental apparatus employed in this thesis. The theory related to bogging including minimum fluidization velocity, bubble diameter and bubble rise velocity in fluidized beds will be presented in Chapter 4. The operation of the agglomerating fluidized bed apparatus and an analysis of the experimental results will be examined in Chapter 5. Finally, the conclusions and recommendations of the study will be summarized in Chapter 6.

CHAPTER 2

Literature Review

The scope of this research was limited to gas fluidized beds operating at ambient temperature which agglomerate due to the addition of a liquid. However, bed agglomeration due to high temperature as well as agglomeration due to liquid deposition are both reviewed in this chapter in order to give a complete perspective. The second section in this chapter will discuss the mathematical methods used to analyze pressure fluctuation signals in this study, including the standard deviation, power spectral density and correlation functions.

2.1 Defluidization

The behavior of fluidized beds in which the size and/or the properties of the fluidized particles change during the process, either due to high temperature or the addition of a liquid to the bed, has not been extensively reported in the fluidization literature. Nevertheless, in many industrial applications, fluidized beds are operated under conditions of pressure and temperature which result in structural or chemical changes on the surface of the fluidized particles which can cause the formation of agglomerates.

Fluidized beds of fine solids are particularly susceptible to the formation of larger size agglomerates if the feed particles are potentially sticky. Commercial fluidized beds tend

to be operated with small sized solids because of their large specific surface area, allowing higher contacting rates. However, this creates problems once stickiness occurs. The stickiness depends on the initial particle size and size distribution, gas pressure, bed geometry, gas humidity, particle surface composition, distributor geometry, and especially the mode of agglomerate formation in the bed. The effect of these conditions on the behavior of the bed is not well understood and has received relatively little attention in the fluidization literature. The basic knowledge in the area is so limited that industry relies mostly on empiricism to avoid defluidization of beds containing sticky particles. Some of the solutions involve changing the operating conditions in the bed to avoid stickiness altogether or adding inert materials to reduce the agglomeration tendency (Tardos *et al.*, 1985).

2.1.1 Defluidization Due to High Temperature

Langston and Stephens (1960) demonstrated how the phenomenon of agglomeration can be harnessed to improve the reduction of iron ore fines to granular metallic iron particles in fluidized beds. Although they did not elaborate on the limits of defluidization, they recognized that the defluidization tendency or the stickiness of the particles is directly proportional to the area of contact, the adhesive property of the particles and inversely proportional to their momentum.

One of the earliest citations of an operating boundary for a bed which could defluidize due to softening and adhesion of the particles at high temperature, a phenomenon known as sintering, was obtained by Goldenberger (1967). He operated an ash agglomerating burner which required successively higher fluidizing velocities to sustain operation at higher temperatures.

In order to study the behaviour of agglomerating beds, Gluckman *et al.* (1976) and Siegell (1976) conducted bench scale experiments at elevated temperatures in which the operating limits of beds of particles that tend to agglomerate by sintering were investigated. In a typical experiment, the bed was fluidized at a given velocity, and the temperature was then increased until defluidization occurred. Defluidization data for a number of solids including copper shot, glass beads, polymeric beads and coal ash were obtained. These investigators found that for a given particle there is a certain gas temperature below which the bed can be fluidized at the minimum fluidization velocity, u_{mf} . Above this threshold temperature, the so-called minimum sintering temperature, T_s, stable fluidization requires correspondingly higher velocities. The velocity and the temperature are in a linear relationship as shown in Figure 2.1.

Gluckman *et al.* (1976) and Sigell (1984) suggested a method to measure the minimum sintering temperature using a dilatometer. This method was further developed and refined by Tardos *et al.* (1984). The particles are placed in a cylindrical sample holder and compressed with a piston. A constant force is applied to the piston and the sample

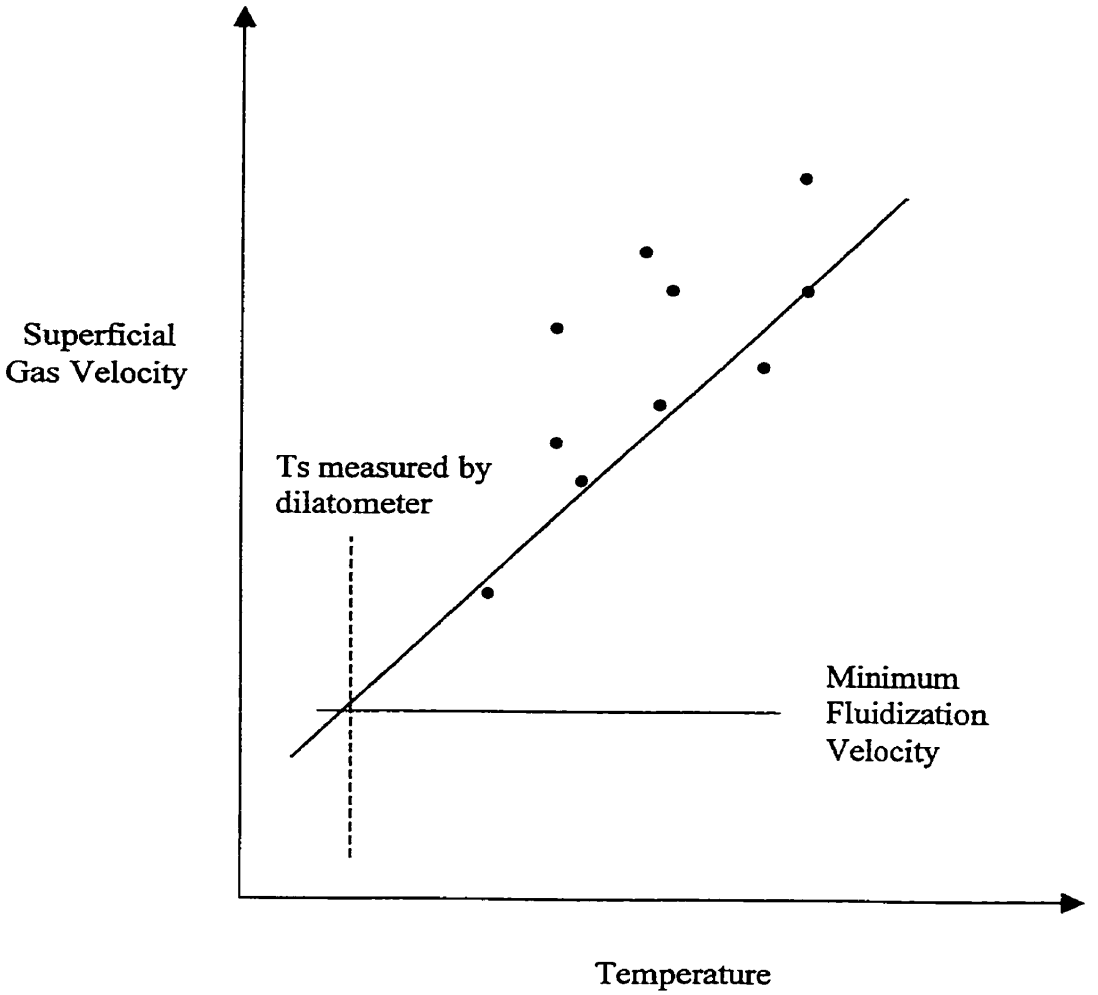

Figure 2.1 Defluidization Limits along with Temperature

(Adapted from Gluckman *et al.*, 1976)

in the cylinder is heated at a programmed rate of temperature rise. The change in length of the sample in the cylinder is plotted as a function of temperature as shown in Figure 2.2. Initially, the particles increase their length linearly with temperature due to thermal expansion. The coefficient of thermal expansion for a particle can be calculated from the slope of the linear portion of the curve before the sintering temperature. At some temperature, which is different for each particle type and size, the slope of the length change curve begins to decrease. This indicates the onset of sintering that is competing with thermal expansion. From this point the slope of the length change curve decreases rapidly until it becomes zero and then continues to decrease and becomes negative. When the slope of the length change curve is zero, the expansion due to thermal effects is just balanced by the contraction due to sintering. This point is the initial sintering temperature T_s.

Gluckman *et al.* (1976) indicated that T_s can also be obtained from the point at which the high temperature defluidization curve intersects the minimum fluidization velocity line, as shown in Figure 2.1.

Gluckman *et al.* (1976) and Siegell (1976) also found that at temperatures above T_s the point of bed defluidization may be determined by observing the pressure drop through the bed. When the bed defluidizes, the material clumps together on the gas distributor blocking the flow of the fluidizing air. Since the forces holding the individual particles together are small compared to the pressure forces of the flowing gas, "rat holes" or

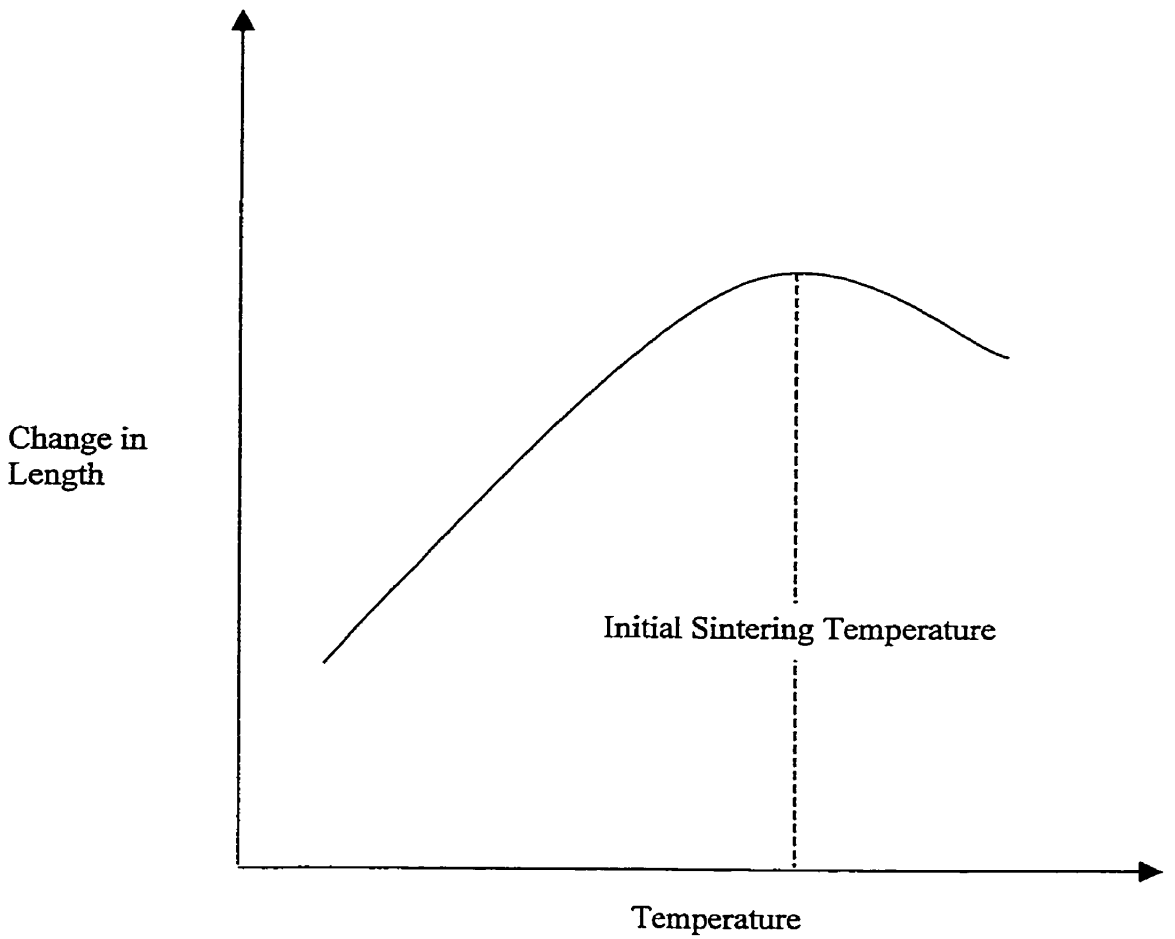

Figure 2.2 Dilatometry Studies on Particles

(Adapted from Gluckman *et al.*, 1976)

"channels" are developed in the bed. The pressure drop through the bed with "rat holes" is substantially less than that of the original fluidized bed, so that bed defluidization is indicated by a sudden decrease in the pressure drop through the bed, as shown in Figure 2.3.

A study by Basu (1982) presents data obtained from an Indian coal ash. Dilatometry measurements were reported and operating boundaries for two different ash samples in the velocity-temperature plane were established. Basu's data confirms the phenomenological picture reported by Sigell (1976) and Gluckman *et al.* (1976).

Liss *et al.* (1983), using the experimental data of Siegell (1976), proposed an expression to compute the limiting gas velocity u_o at high temperature, which is given by:

$$\frac{u_0 - u_{mf}}{u_{mf}} = a\left(\frac{T - T_s}{T_s}\right)^b \tag{2.1}$$

where:

a, b	constants determined from experiments
T_s	minimum sintering temperature, K
u_o	superficial gas velocity, m/s
u_{mf}	minimum fluidization velocity, m/s

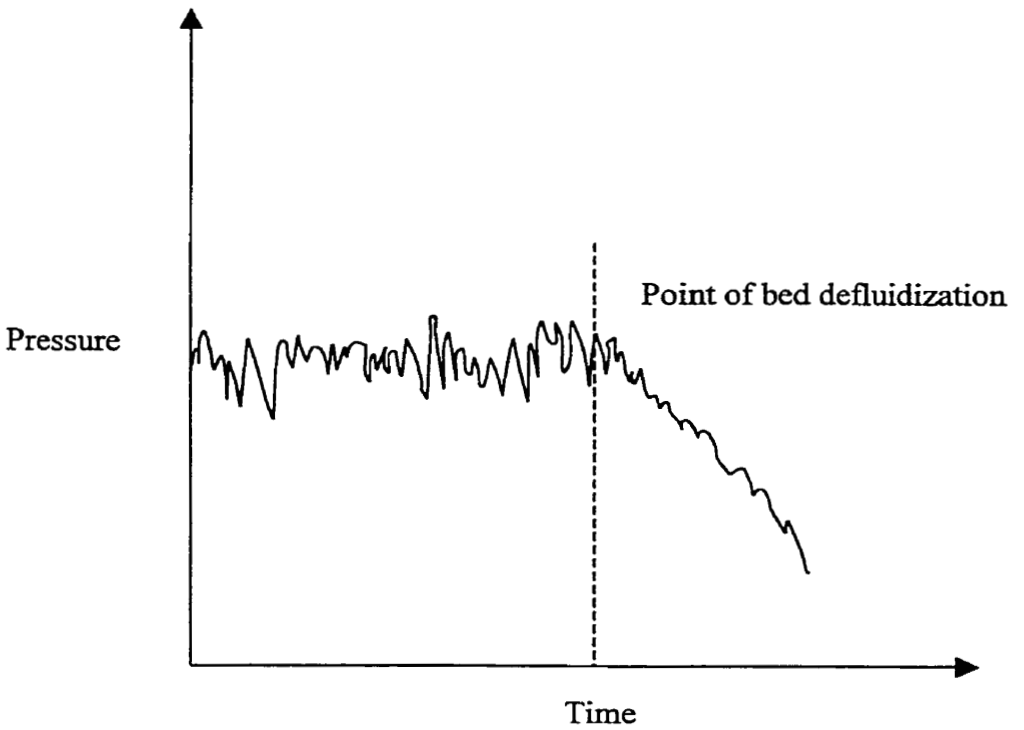

Figure 2.3 Bed Pressure vs. Time for a Defluidization Experiment

(Adapted from Gluckman *et al.*, 1976)

Tardos *et al.* (1985) proposed a theoretical model to predict the limiting gas velocity u_o according to a force balance. At temperature above T_s, besides drag, buoyancy and gravity forces, the adhesive force due to sintering was included in his analysis. This model combined different parameters, including bubble diameter, bed diameter, particle diameter and density, gas density and surface viscosity. Tardos also did experiments to verify his theoretical model.

Other similar models by Harada (1972), Pulvermacher and Ruckenstein (1975) and Kapur (1978) are very useful to predict size distributions, feed and production rates once the predominant mechanisms for particle growth are known and the rate constants required in the models have been measured in pilot scale experiments. These models, however, do not allow for the on-line prediction of agglomerative conditions at which fluidized beds become unstable and defluidization may occur.

2.1.2 Defluidization Due to Liquid Deposition upon the Bed Material

The literature related to defluidization due to liquid deposition is even more scarce than that of defluidization due to high temperature sintering.

Gluckman *et al.* (1976) demonstrated that a nicely fluidized bed suddenly slumped when the quantity of sticky matter added to it exceeded a certain amount. It was observed that the adhesive force between the particles, which is a function of the ratio of the mass of

sticky matter to that of bed material, caused the bed to defluidize as soon as it overcame the momentum of the particles. Therefore, the greater the mass of sticky matter added to the bed, the higher the defluidization tendency, and hence the minimum fluidization velocity.

For bed material, Gluckman used four size cuts of gravitating-bed thermal cracking catalyst and carbon tablets of a single uniform size. As the sticky matter, he used Ace Plastic Coating, #3100 (Ace Glass Vineland, New Jersey). He depicts the defluidization limits for the above particles.

Gluckman concluded that defluidization is a sudden phenomenon – the bed is well fluidized one moment and completely defluidized the next. As the bed defluidizes, the particles become loosely stuck together, and the fluidizing gas blows a hole through the mass of particles to escape. As the hole appears the bed pressure drop decreases dramatically, as shown before in Figure 2.3.

Tardos *et al.* (1985) developed a model which predicts limiting gas velocities necessary to maintain a potentially agglomerating fluidized bed in which a liquid is injected in the bed. He also performed experiments to validate the model.

In his experiments, Tardos used four sizes of TCC catalyst and a liquid coating material (Ace Plastic Coating, #3100, Ace Glass, Vineland, New Jersey) which was sprayed onto

the bed. The total amount of fluid sprayed by the nozzle onto the bed was metered and pressure drop data at a given velocity was recorded until defluidization occurred. Defluidization was observed when the pressure drop through the bed decreased suddenly at which point the particles were no longer supported by the gas stream. He indicated that the limiting velocity was dependent on the amount of liquid added as well as measurable bed and fluid properties.

Most previous studies of bogging have been based on visual observations. The onset of bogging, however, is sometimes very difficult to determine visually. Although Glukman and Siegell indicated that bed defluidization could be detected by a sudden decrease of pressure through the bed, no independent verification of this method has been reported in the literature.

In this study, pressure drop due to bogging was tested by visual observations. As well, different data analysis methods were used to analyze pressure fluctuations in order to find an effective method to detect bogging.

2.2 Analytical Methods of Pressure Fluctuation

The motivation for studying pressure fluctuations is that they give information on the flow of gas in the fluidized bed. As mentioned before, the pressure drop will decrease dramatically due to bogging.

Pressure fluctuations have been used to define an index for the quality of fluidization (Shuster and Kisliak, 1952; Fiocco, 1964; Sutherland, 1964; Winter, 1968). The nature of the pressure fluctuations in a fluidized bed is a complex function of particle properties, bed geometry, pressure and flow conditions of the fluidizing fluid.

A study of the pressure fluctuations in a fluidized bed with on-line measurement and data processing has been found to be efficient with respect to computational effort and to give sufficiently accurate results from the statistical point of view. Pressure fluctuation signals can be employed for calculating bubble size (Lirag and Littman, 1971) and measuring bubble rise velocity (Swinehart, 1966). The analysis of pressure fluctuations for determining their amplitude and frequency could also be a useful way of monitoring changes in bed conditions and for diagnosing abnormalities in bed operation (Fan *et al.*, 1981).

2.2.1 Standard Deviation

The standard deviation of a fluctuating pressure signal is a convenient measurement of fluctuation amplitude.

Some investigators (Cai *et al.*, 1985; Bi and Grace, 1995) used standard deviation to demarcate the onset of the turbulent fluidization regime. Figure 2.4 shows the results of Bi and Grace (1995) for fluid catalytic cracking (FCC) particles of mean size 60 μm.

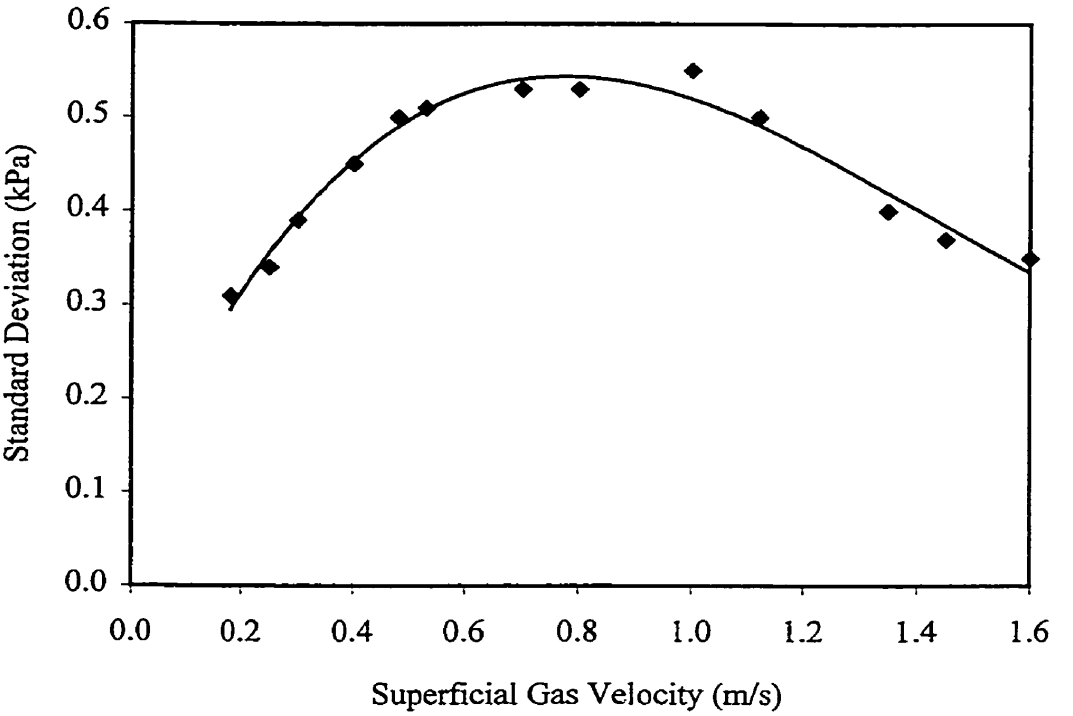

Figure 2.4 Relationship between Standard Deviation and Superficial Gas Velocity (Adapted from Bi and Grace, 1995)

The static bed height was 60 cm and the differential pressure was measured between 3~20 cm.

At low gas velocities, the bed was operating within the bubbling fluidization regime. As the gas velocity was increased, the bubbles grew and coalesced. As a result, the magnitude of pressure fluctuation signal and the calculated standard deviation increased rapidly.

When the gas velocity exceeded a critical point, due to the bubble size and the highly increased break up frequency of the bubbles, the bed was transformed from the bubbling to the turbulent fluidization regime. At this time, it could be noted that the standard deviation of signals was reduced gradually, and a maximum appeared in the curve of standard deviation versus gas velocity. This peak corresponded to the transition from bubbling to turbulent fluidization.

2.2.2 Correlation Function and Power Spectral Density Function

Among the various statistical parameters associated with random processes two stand out as being of significant importance, namely, the correlation function and the spectral density function (Bendat, 1977). The correlation function gives the degree of coherence of two time series and the spectral density function is the Fourier transform of a correlation function.

Pressure fluctuation analysis has been used in three-phase fluidized systems by Fan et al. (1986) and Jakher (1998) as an effective technique for flow regime identification. This technique requires the use of transducers with fast response times and an evaluation of the statistical properties of the wall pressure fluctuations, specifically the power spectral density function. The power spectral density function (PSDF) expresses the distribution of energy with frequency and is calculated by the Fourier transform. It was observed by Fan *et al.* (1986) that the PSDF has a distinct pattern for each flow regime.

The equations and explanations of the above functions will be presented in the next chapter. Details of the statistical analysis of random functions can be found in Bendat (1977), Brown and Nilsson (1962), Crandall and Mark (1963), Davenport and Root (1958), Lee (1960) and Stearns (1975).

It is postulated that the bogging phenomena is similar to a regime transition to some extent. Therefore, in this study, all of the above methods were used to analyze bed pressure drop to discern the variations in pressure fluidizations due to particle agglomeration from those due to gas bubbles and turbulence.

CHAPTER 3

Theory

This chapter gives an overview of the basic theory related to agglomerative fluidization. As mentioned in Chapter 2, the bed pressure drop decreases due to particle agglomeration. In fluidized beds, the pressure fluctuations are related to bubble size and movement. In this chapter, the minimum fluidization velocity, bubble diameter, bubble rise velocity and analytical methods will be described in detail.

If a fluid is passed upward through a bed of fine particles at a low flow rate, the fluid merely percolates through the void spaces between stationary particles. This is the fixed bed regime. With an increase in flow rate, particles move apart and a few vibrate and move in restricted regions. This is the expanded bed regime (Kunii and Levenspiel, 1991).

At a still higher velocity, a point is reached where all the particles are just suspended by the upward flowing fluid. At this point the frictional force between particles and fluid just counterbalances the weight of the particles, the vertical component of the compressive force between adjacent particles disappears, and the pressure drop through any section of the bed about equals the weight of fluid and particles in that section. The bed is considered to be incipiently fluidized, a condition referred to as minimum fluidization (Kunii and Levenspiel, 1991).

For gas-solid systems, with an increase in flow rate beyond minimum fluidization, large instabilities with bubbling and channelling of gas are observed. At higher flow rates, agitation becomes more violent and the bed does not expand much beyond its volume at minimum fluidization. This conditionis called the bubbling fluidization regime. Gas bubbles coalesce and grow as they rise (Kunii and Levenspiel, 1991).

3.1 Solids with a Distribution of Sizes

If fluid beds contain solids of different sizes, it is convenient to use a mean diameter $\overline{d_p}$ to evaluate the behaviour of particles.

$$\overline{d_p} = \frac{1}{\sum\left(\frac{x_i}{d_{pi}}\right)} \tag{3.1}$$

where:

x_i weight fraction of material in size interval i

d_{pi} particle diameter in size interval i, m

3.2 Minimum Fluidization Velocity, u_{mf}

u_{mf} is the superficial gas velocity at minimum fluidizing conditions. It is the most important measurement needed for design. Numerous correlations have been proposed for its prediction, the most famous being the Ergun Equation (1952).

For small particles, the Ergun Equation can be simplified to the following equation.

$$u_{mf} = \frac{d_p^{\,2}(\rho_s - \rho_g)g}{150\mu_g}\frac{\varepsilon_{mf}^{\,3}\phi_s^{\,2}}{1-\varepsilon_{mf}} \tag{3.2}$$

where:

d_p	particle diameter based on screen analysis, m
ρ_s, ρ_g	density of solids and air, kg/m^3
μ_g	air viscosity, kg/m s
ε_{mf}	void fraction in a bed at minimum fluidizing condition, dimensionless
ϕ_s	sphericity of particles, dimensionless
u_{mf}	minimum fluidization velocity, m/s

3.3 Bubble Size

Toomey and Johnstone (1952) proposed an elegant two-phase model that successfully accounted for the movement of both gas and solids and the pressure distribution about rising bubbles. This model is a significant breakthrough because of its simplicity and essential correctness. In this model the fluidized bed is considered to consist of two distinct phases; the bubble phase containing little or no solids, and the emulsion or dense phase containing the majority of the solids.

The two-phase model shows that in bubbling beds roughly all gas in excess of that needed to just fluidize the bed passes through the bed as bubbles, and the emulsion phase remains close to minimum fluidizing conditions. There is also an interchange of gas between the bubble and dense phase in fluidized beds.

These findings show that a bed at minimum fluidizing conditions can be treated as a liquid of low or negligible viscosity. At higher velocity the excess gas goes through the bed as bubbles, which rise as in an ordinary liquid of low viscosity. The voidage of a bed, not counting bubbles, remains close to ε_{mf}. At minimum fluidizing conditions, the solids are relatively quiescent. At higher gas velocities the rising bubbles cause the observed churning, mixing and flow of solids.

An equation describing the bubble diameter just above the distributor is given by Kunii and Levenspiel (1991).

$$d_{b0} = \frac{2.78}{g}\left(u_0 - u_{mf}\right)^2 \tag{3.3}$$

where:

d_{bo} bubble diameter just above the distributor, m

u_o superficial gas velocity, m/s

Werther (1978) gives the following expression for bubble size at any height z in a bed.

$$d_b = 0.853\left[1 + 0.272\left(u_0 - u_{mf}\right)\right]^{1/3}\left(1 + 0.0684z\right)^{1.21} \tag{3.4}$$

where:

d_b bubble diameter, m

3.4 Bubble Rise Velocity

On the basis of simple two-phase theory, Davidson and Harrison (1963) proposed the following rise velocities.

For single bubbles:

$$u_{br} = 0.711(gd_b)^{0.5} \tag{3.5}$$

For bubbles in bubbling beds:

$$u_b = u_0 - u_{mf} + u_{br} \tag{3.6}$$

where:

u_{br} bubble rise velocity with respect to the emulsion phase, m/s

u_b bubble rise velocity, m/s

Based on the above equations, Werther (1983, 1986) did extensive experimental work and proposed the following equations which also account for the vessel size.

For Geldart A solids

$$u_b = 1.55\left[(u_0 - u_{mf}) + 14.1(d_b + 0.005)\right]d_t^{0.32} + u_{br} \tag{3.7}$$

For Geldart B solids

$$u_b = 1.6\left[(u_0 - u_{mf}) + 1.13d_b^{0.5}\right]d_t^{1.35} + u_{br} \tag{3.8}$$

where:

d_t bed diameter, m

From Equation 3.2, it is shown that as the particle diameter or particle density increases, the minimum fluidization velocity will increase. The effect of particle diameter is much greater than that of particle density because the minimum fluidization velocity varies asthe square of the particle diameter.

When u_{mf} increases, the above equations indicate that both bubble diameter and bubble rise velocity will decrease. The bubbles in the bed will be smaller and vibrate slightly. Therefore the amplitude of pressure fluctuation through the bed is expected to decrease.

$$d_p \uparrow \text{ or } \rho_s \uparrow \;\rightarrow\; u_{mf} \uparrow \;\rightarrow\; d_{b0} \downarrow, d_b \downarrow \;\rightarrow\; u_b \downarrow$$

3.5 Standard Deviation

Standard deviation describes the deviation of each individual pressure measurement from the average pressure. Standard deviation reflects the amplitude of pressure fluctuation directly.

The mean value, mean square value and variance of a random process x(t) are given as:

$$\mu = \lim_{T \to \infty} \frac{1}{T} \int_0^T x(t)dt \tag{3.9}$$

$$\varphi^2 = \lim_{T \to \infty} \frac{1}{T} \int_0^T x^2(t)dt \tag{3.10}$$

$$\sigma^2 = \lim_{T \to \infty} \frac{1}{T} \int_0^T (x(t) - \mu)^2 dt \tag{3.11}$$

where:

μ	mean value
φ^2	mean square value
σ^2	variance
T	period of sampling, s

The positive square root of the variance is called the standard deviation.

3.6 Correlation and Spectral Density Functions

The covariance function assesses the degree of linear dependence between two random variables, x(t) and y(t). It is the average product of $x(t) - \mu_x$ and $y(t) - \mu_y$. The covariance function between x(t) and y(t) for any time delay τ is given by:

$$C_{xy}(\tau) = \lim_{T\to\infty} \frac{1}{T} \int_0^T (x(t) - \mu_x)(y(t+\tau) - \mu_y)dt = R_{xy}(\tau) - \mu_x \mu_y \tag{3.12}$$

where:

$$R_{xy}(\tau) = \lim_{T\to\infty} \frac{1}{T} \int_0^T x(t) y(t+\tau) dt \tag{3.13}$$

C_{xy}	cross-covariance function
R_{xy}	cross-correlation function

For the special case where y(t)=x(t), the auto-covariance function is:

$$C_{xx}(\tau) = \lim_{T\to\infty} \frac{1}{T} \int_0^T (x(t) - \mu_x)(x(t+\tau) - \mu_x)dt = R_{xx}(\tau) - \mu_x^{\ 2} \tag{3.14}$$

where:

$$R_{xx}(\tau) = \lim_{T\to\infty} \frac{1}{T} \int_0^T x(t) x(t+\tau) dt \tag{3.15}$$

C_{xx}	auto-covariance function
R_{xx}	auto-correlation function
τ	time shift variable
T	period of sampling, s
x(t), y(t)	random variables

From Equations 3.9 to 3.11, the value of the auto-correlation function and auto-covariance function at $\tau = 0$ is the mean square value of the data and variance of the data respectively.

$$R_{xx}(0) = \varphi_x^{\ 2} \tag{3.16}$$

$$C_{xx}(0) = \sigma_x^{\ 2} \tag{3.17}$$

The spectral density function between two time history records x(t) and y(t) is defined as follows:

$$S_{xy}(f) = \int_{-\infty}^{\infty} R_{xy}(\tau) e^{-j2\pi f\tau} d\tau \tag{3.18}$$

For the general case where x(t) and y(t) represent different data, $S_{xy}(f)$ in Equation 3.18 is called the cross-spectral density function, or more simply the cross-spectrum, between x(t) and y(t). For the special case where y(t)=x(t):

$$S_{xx}(f) = \int_{-\infty}^{\infty} R_{xx}(\tau) e^{-j2\pi f\tau} d\tau \tag{3.19}$$

where $S_{xx}(f)$ is called the autospectral density function or autospectrum of x(t). This function is also commonly known as the power spectral density function because of its historical origin and use in communications engineering applications (Bendat and Piersol, 1993).

CHAPTER 4

Experimental Apparatus and Methods

This chapter outlines the experimental apparatus and verification of experimental methods. Figure 4.1 shows a photo of the experimental apparatus and Figure 4.2 is a schematic diagram.

4.1 The Column

The column was made of Plexiglas to aid in visual observation of the phenomena in the bed. A diagram of the column with dimensions is given in Figure 4.3. The section above the distributor was made of Plexiglas of 15 cm I.D. and 150 cm length. One pressure transducer was connected to the very bottom of the bed in order to measure the total bed pressure drop. Another pressure transducer was placed near the top of the column to detect the pressure fluctuations in the air above the bed. A grounded iron coil with aluminium foil was wrapped around the bed to prevent the build up of static electricity. The pressure ports were equipped with size 200 stainless steel wire mesh located inside the column wall to prevent the pressure transducers from being clogged with particles. An experiment was conducted that showed the pressure drop through mesh to be very small, and of the order of resolution of the data acquisition board. The effect of the mesh on the pressure signal can therefore be neglected.

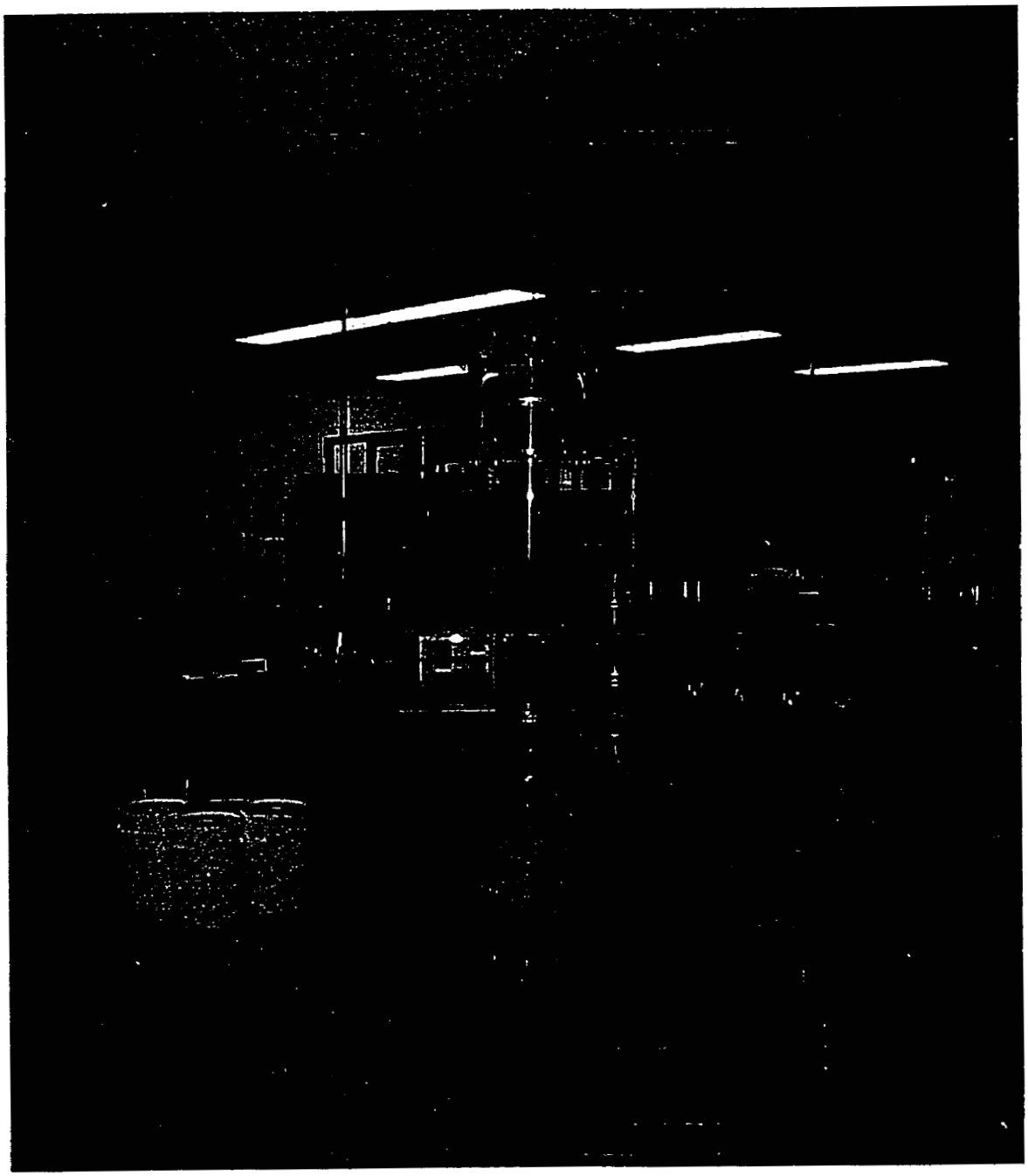

Figure 4.1 Photo of Experiment Apparatus

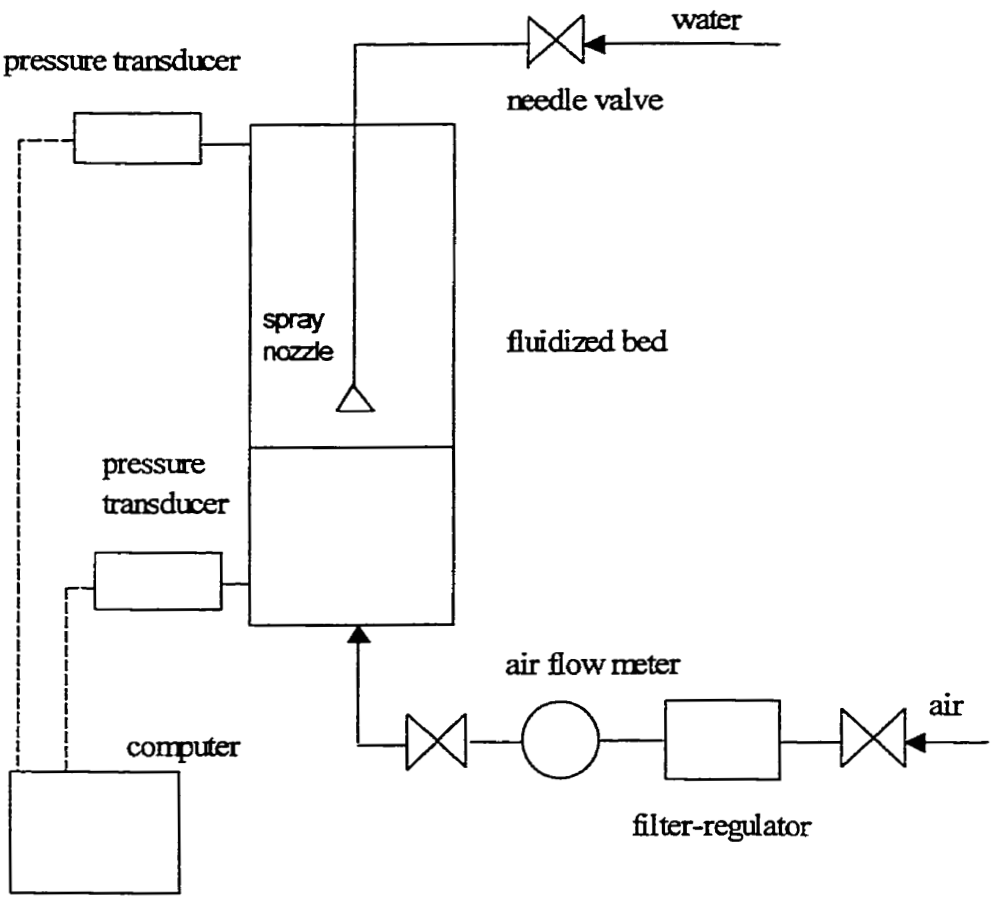

Figure 4.2 Schematic Diagram of Experimental Apparatus

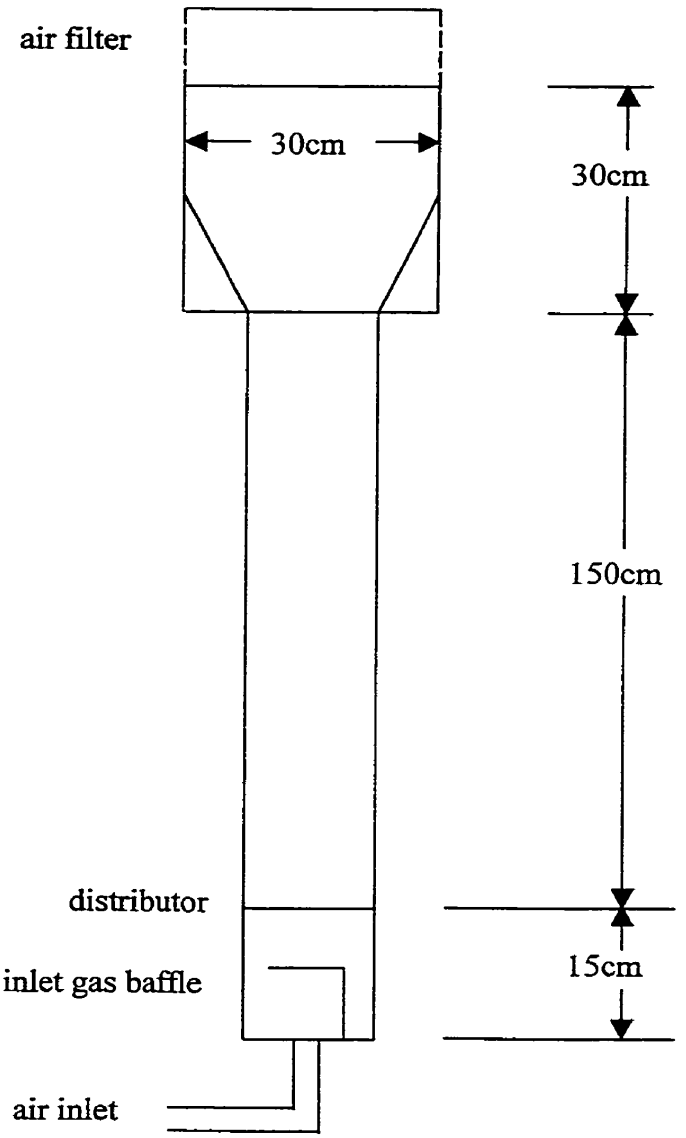

Figure 4.3 Column with Dimensions

The section below the distributor was 15 cm I.D. and 15 cm length. A baffle was located at the bottom of the tube in order to distribute the air. The perforated plate distributor had 90 orifices of 1 mm diameter on a square pitch. A layer of 200 stainless steel wire mesh was used above the distributor to prevent particle leakage. The entire distributor arrangement was connected to the bed by flanges to facilitate removal for cleaning.

The disengagement section was a 30 cm I.D., 30 cm length Plexiglas pipe located at the top of the column which allowed the gas and particles to separate. An automotive air filter was placed on the top of disengagement section in order to prevent the emission of fine particles.

4.2 Air Supply

Air was obtained from the building supply at 550 kPa pressure. The air was filtered to remove oil, water and small particles and regulated using a combined filter-pressure regulator (supplied by Century Sales & Service Ltd., ARO-P29241-100). A pressure gauge was placed upstream of the filter-regulator to read the supply pressure. The air flow rate was monitored using an Omega FL-7918 air rotameter. The rotameter was calibrated using a "bell prover" consisting of a large bell shaped float immersed in an oil bath. Building air was passed through the rotameter and into the oil bath, displacing the float. The rate at which the float rises indicates the volumetric flow of the gas into the

oil bath, and hence the volumetric flow of air at the particular rotameter setting. The calibration diagram of rotameter is given in Appendix A. A brass valve was placed at the rotameter outlet to control the air flow being fed to the column. Half-inch nycoil air line (Century Sales & Service Ltd.) was used before and after the rotameter.

4.3 Water Supply

Water was sprayed into the bed in order to cause bed agglomeration. Experiments using different particles with water were done to observe and investigate bogging phenomena.

A brass 5 mm I.D. flowline was connected from the lab supply to the centre line of the bed. A spray atomizing nozzle (John Brooks Co. Ltd. model 1/4 LN 18) was located at the end of the flowline. The tip of the nozzle was located approximately 10 cm above the static bed. When the bed fluidizes, the nozzle merges into the fluidized particles. This minimizes water vaporization into the air and particle adhesion on the bed wall. The water flow rate to the column was measured with a calibrated needle valve. A calibration curve for the needle valve is included in Appendix B. After each experiment, the flow of water was stopped and the bed was fluidized until the bed material was totally dry.

4.4 Pressure Transducers and Data Acquisition System

Two SRP Control Systems pressure transducers (model PT 420) were used during the experiments. These pressure transducers have a 2 kHz response time, $\pm$ 0.2% accuracy, and a range of 0-34.5 kPa. Acquisition of the pressure signals was performed using a 12-bit National Instruments board (PC-LMP-16), connector block (CB-50LP) and cable (NB1). Power for the pressure transducers was supplied by an Omega power supply (U24Y101). The software package LabView was used to record the raw pressure fluctuation data on the computer.

4.5 Solid Particles

Different particles were used in this work. According to the Geldart Classification of particles, three groups were included:

Group A: FCC (Fluid Catalytic Cracking) catalyst

Group B: two kinds of sand and polystyrene

Group D: glass beads

A sieve analysis was performed to determine the mean particle diameter of the different kinds of particles. The cumulative mass fraction distribution curve for different particles can be found in Appendix C. The particle density was determined from a standard

procedure whereby the volume of water displaced by a known mass of particles was measured. The bulk density was determined from the weight of a dry sample of particles in a graduated cylinder. The packed bed voidage is simply one minus the ratio of the bulk density to the particle density. The bed height at minimum fluidizing conditions was measured and the minimum fluidization voidage was calculated. A sphericity of one was assumed for all particles. The Ergun Equation (1952) was used to calculate the minimum fluidizing velocity u_{mf} (Equation 3.2). Finally, the terminal velocities of different particles were calculated from the correlation of Haider and Levenspiel (1989), Equations 4.1 to 4.3. The physical properties are summarized in Table 4.1.

$$d_p^* = d_p \left[\frac{\rho_g (\rho_s - \rho_g) g}{\mu_g^2} \right]^{\frac{1}{3}} \tag{4.1}$$

$$u_t^* = \left[\frac{18}{(d_p^*)^2} + \frac{2.335 - 1.744\phi_s}{(d_p^*)^{0.5}} \right]^{\frac{1}{3}} \tag{4.2}$$

$$u_t = u_t^* \left[\frac{\mu (\rho_s - \rho_g) g}{\rho_g^2} \right]^{\frac{1}{3}} \tag{4.3}$$

Table 4.1 Physical Properties of Particles

	FCC	Smaller Sand	Larger Sand	Glass Beads	Polystyrene
Mean Diameter (μm)	91	281	574	5000	1319
Particle Density (kg/m^3)	1343	2581	2555	2524	974
Bulk Density (kg/m^3)	990	1650	1719	1486	635
Packed Bed Voidage	0.26	0.36	0.33	0.41	0.35
Minimum Fluidization Velocity (m/s)	0.0017	0.0789	0.2456	37.93	0.5974
Minimum Fluidization Voidage	0.31	0.40	0.37	0.45	0.39
Terminal Setting Velocity (m/s)	0.28	2.47	4.76	17.02	4.95

where:

d_p	particle diameter based on screen analysis, m
ρ_s, ρ_g	density of solids and air, kg/m^3
μ_g	air viscosity, kg/m s
ϕ_s	sphericity of particles, dimensionless
u_t	terminal settling velocity, m/s

4.6 Verification of Experimental Methods

Accurate measurement of pressure fluctuations was critical in the experimental investigations. A number of different techniques have been used and tested to determine the accuracy of the pressure fluctuation measurements.

4.6.1 Sampling Frequency

Many previous investigators have used a sampling frequency of 100 Hz to record pressure fluctuations in fluidized beds (Satija and Fan, 1985; Fan *et al.*, 1986; Bi and Grace, 1995; Jakher, 1998). In this work, 100 Hz was used in all experiments. A TEK 224 digital storage oscilloscope was used to determine if this sampling frequency was sufficiently high. With the bed in operation, the oscilloscope sampled the signal from the lower pressure transducer at a frequency of 7.5 MHz. This oscilloscope trace was then compared to the pressure fluctuation signal gathered using the data acquisition

board at 100 Hz sampling frequency. The results were very similar except for a low amplitude noise signal, confirming that no important information was lost at a sampling frequency of 100 Hz.

4.6.2 Response Time

In order to accurately measure the rapidly fluctuating pressures in the fluidized bed, the response time of the pressure transducer must be very short. According to the manufacturer's specifications, the pressure transducers used in this study have a response time of 2 kHz. As the sampling frequency of 100 Hz is much less than 2 kHz, the acquired pressure signal was assumed to be equal to the pressure signal at the wall of the column. The response time of the pressure transducer is rapid enough so as not to limit the accuracy of the instantaneous pressure fluctuation data.

4.6.3 Noise Fluctuation

An experiment was performed using FCC particles. The static bed height was 30 cm, the superficial gas velocity was 0.04 m/s and the run time was 60 seconds. Two pressure transducers were connected to the fluidized bed; one at the very bottom of the bed to measure the total bed pressure drop, and another at the top of the bed to measure the pressure fluctuation due to air leaving the bed. From Fig 4.4, it is indicated that the amplitude of the upper transducer is much less than that of lower transducer. The

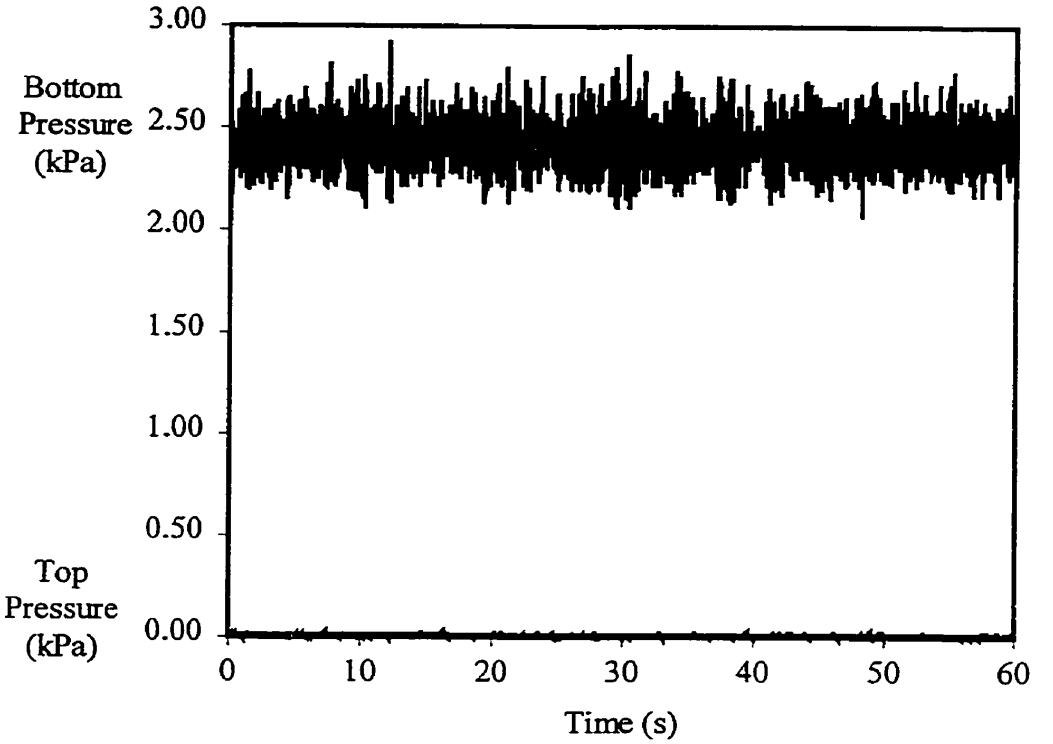

Figure 4.4 Pressure Fluctuations Measured by Top and Bottom Pressure Transducers

average value of bottom transducer was 2.42 kPa while the top one was 0.01 kPa. Therefore pressure measured at the lower transducer was assumed to be sufficient for characterizing the pressure fluctuations occurring the bed.

4.6.4 Experimental Comparison

An experiment was done with FCC particles with a static bed height of 26 cm. With the bed operating in the bubbling regime, the signal from the lower pressure transducer was recorded for 60 seconds and the average standard deviation calculated. The average standard deviation as a function of the superficial gas velocity is shown in Figure 4.5.

Comparing this figure with the data of Bi and Grace (1995) of Figure 2.4, it is shown that the pressure signals have the same trend and similar value. The standard deviation value in Figure 4.5 is slightly lower than that of in Figure 2.4 because FCC particles in Bi and Grace experiments have smaller mean diameter. In this study, the air supply was insufficient to cause the transition from the bubbling to the turbulent fluidization regime, so the curve in Figure 4.5 does not display a maximum value observed by Bi and Grace. However, the data within the bubbling regime is similar in both studies. Therefore, we have confidence that our apparatus provides similar data to that produced by other researchers.

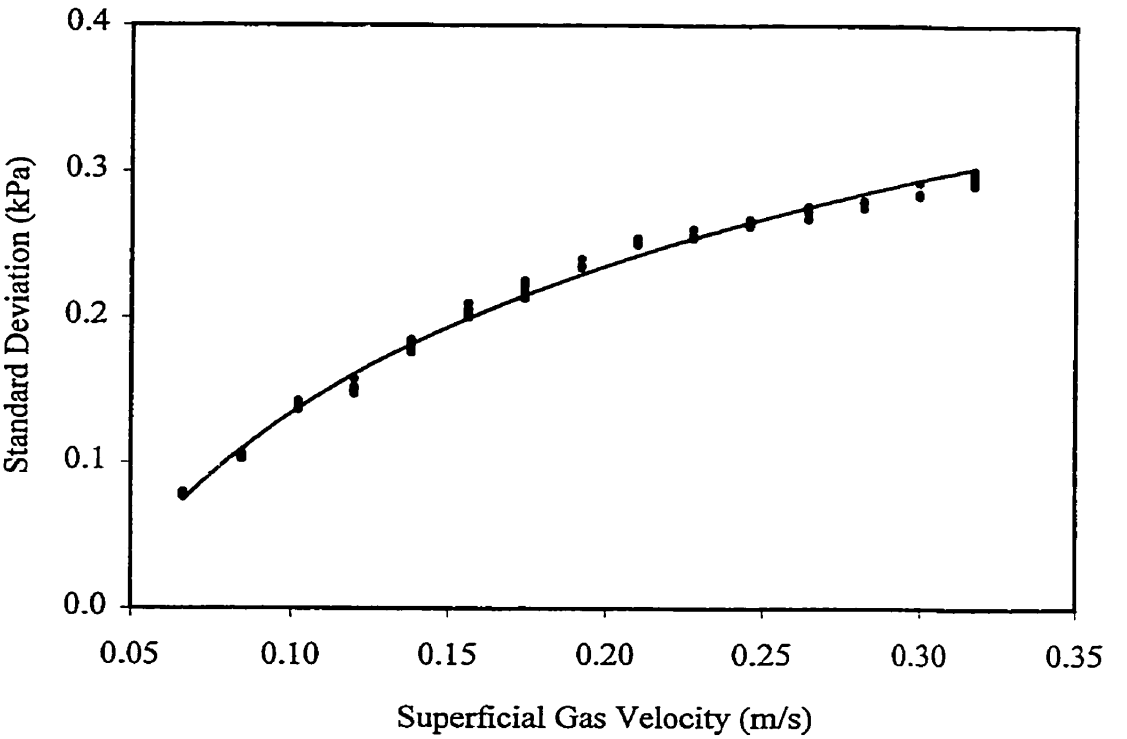

Figure 4.5 Relationship between Standard Deviation and Superficial Gas Velocity

Chapter 5

Results and Discussion

In this study, Group A (FCC) and Group B (sand) particles were used during experiments to observe bogging phenomena for different solids. Pressure fluctuations were measured in a fluidized bed. The measurements were made very close to the distributor, and were therefore equal to the total pressure drop across the fluidized bed.

The standard deviation function, power spectral density function and autocovariance function were used to analyze pressure fluctuation signals in order to detect the onset of bogging.

Two main sets of experiments were performed. In the first set, particle agglomeration was achieved by wetting the bed material with water. Water was sprayed from the nozzle onto particles to simulate agglomerative fluidization behavior of units such as a fluid coker. Bogging phenomena were visually observed and pressure signals were analyzed. The second set of experiments utilized large diameter solids which were introduced into a bed of smaller particles to simulate particle agglomeration.

Table 5.1, Table 5.2 and Table 5.3 give the summary of all the experiments conducted. Five typical experiments will be explained in detail in the following sections.

Table 5.1 Summary of Experiments Using FCC

	Date	Static Bed Height (cm)	Superficial Gas Velocity (m/s)	Water Flow Rate (g/s)	Experiment Content	Total Run Time (s)
1	99-12-22	30	0.04		Use 906g polystyrene instead of FCC	60
2	99-12-20	30	0.07	4	t=20s sprayed water	200
3	99-12-17	30	0.04	3	t=20s sprayed water	200
4	99-09-18	30	0.04	2	t=25s sprayed water	250
5	99-09-17	30	0.04	2	t=20s sprayed water, t=40s stopped water and t=100s sprayed water again	250
6	99-09-15	30	0.04	3	t=20s sprayed water, t=60s stopped water and t=100s sprayed water again	250
7	99-09-14	30	0.04	3	t=20s sprayed water, t=60s stopped water and t=80s sprayed water again	250
8	99-09-12	30	0.04	3	t=25s sprayed water	250

Table 5.2 Summary of Experiments Using Smaller Sand

	Date	Static Bed Height (cm)	Superficial Gas Velocity (m/s)	Water Flow Rate (g/s)	Experiment Content	Total Run Time (s)
1	99-11-29	30	0.16	2	t=20s sprayed water	120
2	99-11-26	30	0.25	2	t=20s sprayed water	120
3	99-11-24	30	0.25	1	t=20s sprayed water	90
4	99-11-21	30	0.25		Use 1680g larger sand instead of smaller sand	60
5	99-11-09	30	0.25		Use 193g glass beads instead of smaller sand	60
		30	0.25		Use 810g glass beads instead of smaller sand	60
		30	0.25		Use 1217g glass beads instead of smaller sand	60
		30	0.25		Use 1777g glass beads instead of smaller sand	60

Table 5.3 Summary of Experiments Using Larger Sand

	Date	Static Bed Height (cm)	Superficial Gas Velocity (m/s)	Water Flow Rate (g/s)	Experiment Content	Total Run Time (s)
1	99-09-27	12	0.43	0.54	t=60s sprayed water	200
2	99-09-25	12	0.61		0-60s, no beads 60-90s, 100g beads 90-120s, 200g beads 120-150s, 500g beads 150-180s, 800g beads	180
3	99-09-23	12	0.61	0.54	t=60s sprayed water	200

5.1 Defluidization of Group B Materials

In this section, the results of three main experiments are presented. The first set of experiments examined sand agglomerated with water, the second involved a mixture of sand having different particle sizes, and the third involved a mixture of sand and large diameter glass beads. Pressure fluctuations were recorded and analyzed respectively.

5.1.1 Sand Agglomerated with Water

Sand having a mean particle diameter of 281 μm was used in this experiment. The static bed height was 30 cm, and the superficial gas velocity was 0.25 m/s. The computer recorded the pressure fluctuation signals. After 20 seconds of operation, the needle valve was opened and water was sprayed onto particles at a rate of 2 g/s. The raw pressure data was sampled at a rate of 100 Hz continuously until 120 seconds total operating time.

Fig 5.1 shows the pressure fluctuation with time. It is clear that the total pressure drop decreases, and the amplitude of pressure fluctuation decreases as well.

The moving average pressure drop was calculated using an interval of 100 data points. Each point on Fig 5.2 represents the average value of last 100 pressure measurements. It is shown that between 0-20 seconds, pressure fluctuates normally, representing fluidized

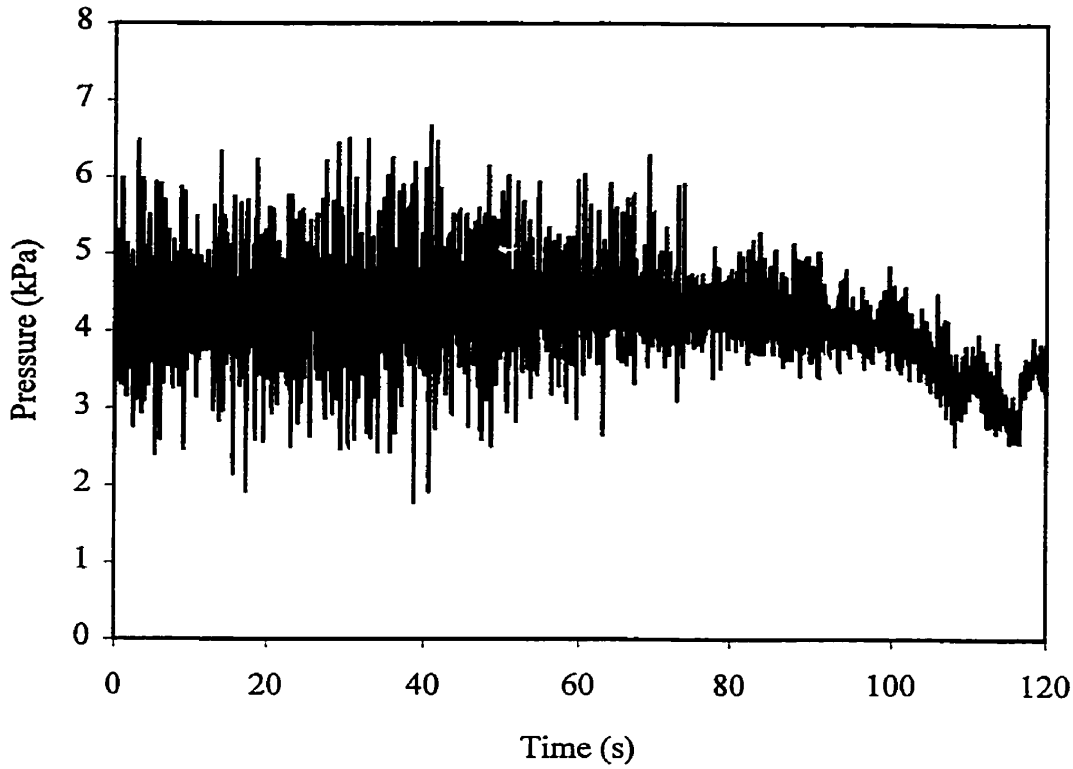

Figure 5.1 Pressure Fluctuation with Time for Sand-Water System

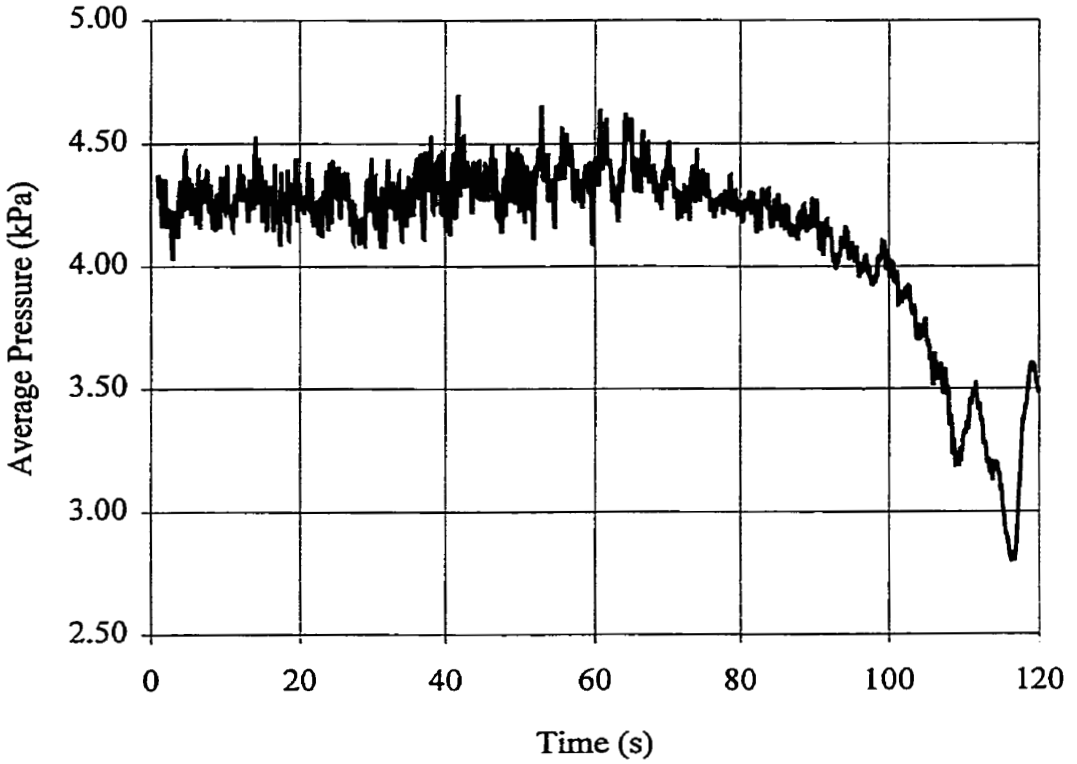

Figure 5.2 Average Pressure with Time for Sand-Water System

dry sand; between 20-60 seconds, the pressure increases continuously due to the increased mass of the bed caused by the introduction of the water. In a well-fluidized bed, the pressure should be proportional to the total mass in the bed, the more water, the higher the pressure. Table 5.4 shows that the observed pressure increase is approximately equal to the mass of water added up to the point at which the bed bogs and fluidization is lost. Therefore, water loss due to evaporation and adhesion to the column wall is virtually negligible.

Table 5.4 Water Balance for Sand-Water System

Water sprayed between 20-60 s, g	80
Total water weight G = mg, N	0.7848
Average Pressure at 20 s, kPa	4.2928
Average Pressure at 60 s, kPa	4.3376
Pressure increase between 20-60 s, kPa	0.0448
F = P×A (bed cross section area), N	0.7919

G (water weight) ≈ F (pressure increase measured by pressure transducer)

After about 60 seconds, the pressure decreases dramatically. This observation agrees with that of Gluckman. As the bed defluidizes the particles become loosely stuck

together, and channels develop in the bed material allowing the fluidizing gas to escape. As the channels appear, the bed pressure drop decreases dramatically. Gluckman (1976) concluded that the bed pressure drop decrease is a good indication of the "sharpness" of the defluidization. However, from visual observations it was apparent that some channels had developed after only approximately 40 seconds. After 60 seconds a large number of channels were observed indicating that the wetted sand had already undergone substantial agglomeration. It is therefore concluded that the pressure drop decrease took place only after substantial bogging had occurred and that the pressure decrease cannot be used as a reliable indication of the onset of bogging.

While the total bed pressure drop did not provide an indication of the onset of bed agglomeration, it is possible that changes in the pressure fluctuation signals can provide a more reliable indicator of the onset of bogging.

In Figure 5.1, it is shown that the amplitude of the pressure decreases as more and more water is sprayed into the bed. The standard deviation function provides a direct indication of the change in pressure fluctuation amplitude. Figure 5.3 shows the change in the moving standard deviation function with time. The standard deviation was calculated over an interval of 100 points, or 1 second operating time. It is shown that after about 40 seconds, the standard deviation decreases continuously, corresponding to the visual observation of the first appearance of channels in the bed. Therefore the

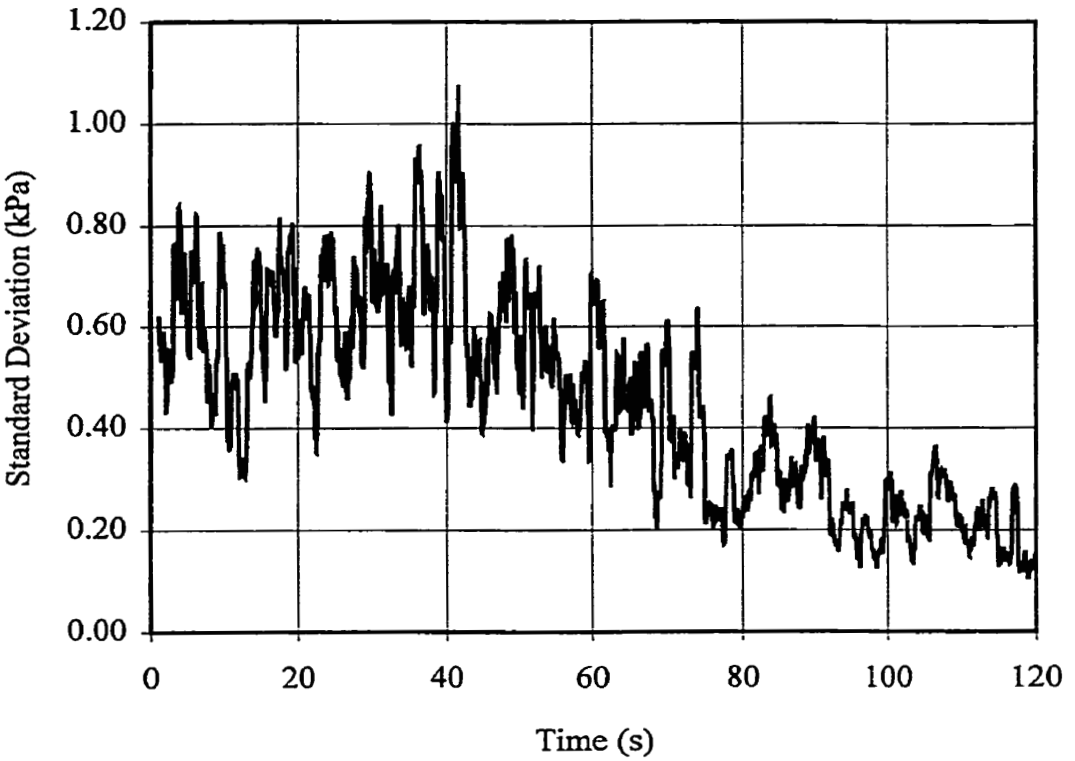

Figure 5.3 Standard Deviation of Pressure with Time for Sand-Water System

standard deviation function gives a more reliable indication of the onset of bed agglomeration than the overall bed pressure drop.

The power spectral density function (PSD) has been shown by other researchers to be a good method of identifying flow regimes for liquid fluidized systems. It is therefore sensible that the PSD may also provide an indication of bed agglomeration. In this work the software package Matlab was used to calculate the PSD of the pressure signal. The Matlab PSD routine employed a Hanning window in order to provide a more accurate estimate of the actual underlying spectrum. The ensemble average PSD was calculated using 256 points and the length of the Hanning window was 256 points. Three curves are presented in Figure 5.4; the PSD for the dry fluidized particles prior to the introduction of water to the bed (0-20s), and the PSD for wetted particles for the time periods 20-40s and 40-60s. After 60 seconds operating time, the bed became completely defluidized, therefore the PSD of the pressure signal after 60 seconds operating time was not included in this figure. From Figure 5.4, it is shown that all three curves are almost the same, showing that the PSD function does not give any indication of bogging. It is apparent that the change in the behavior of the bed due to particle agglomeration is not the same as that which occurs during the transition between flow regimes.

Figure 5.5 shows the PSD function over 1 second. The calculation period (100 point) is the same as that of the moving average pressure and moving standard deviation. As shown in this figure there is no apparent difference before and after bogging.

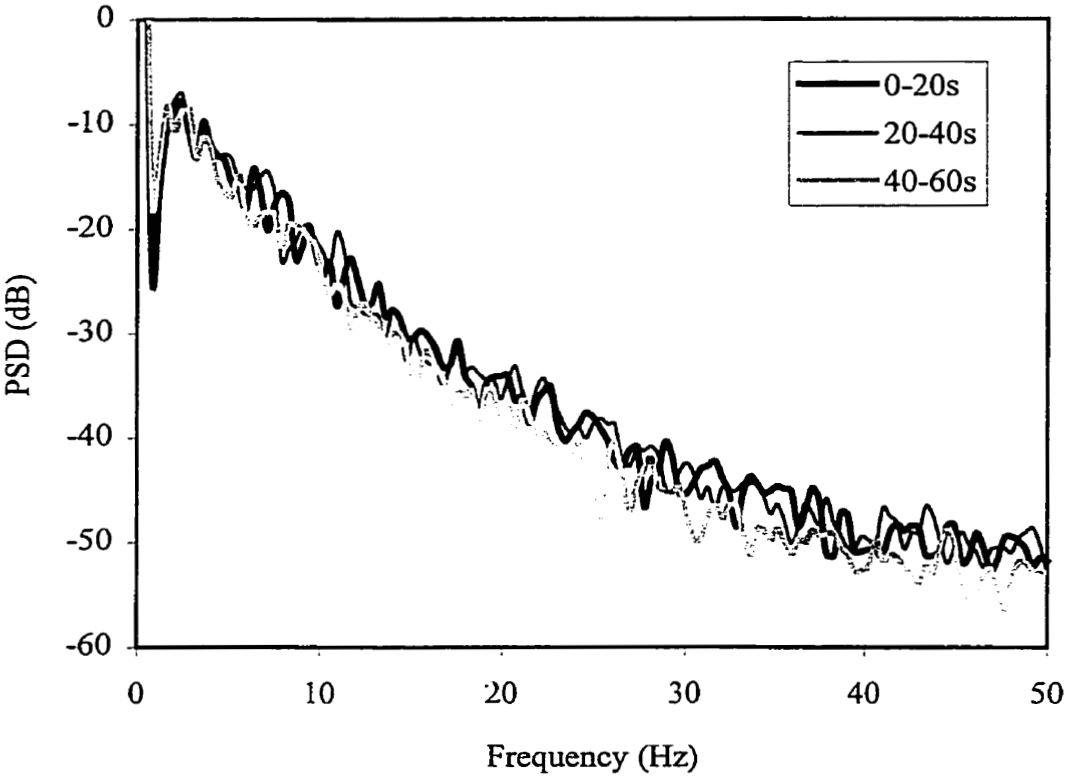

Figure 5.4 Power Spectral Density Function of Different Time Zone for Sand-Water System (20 s calculation period)

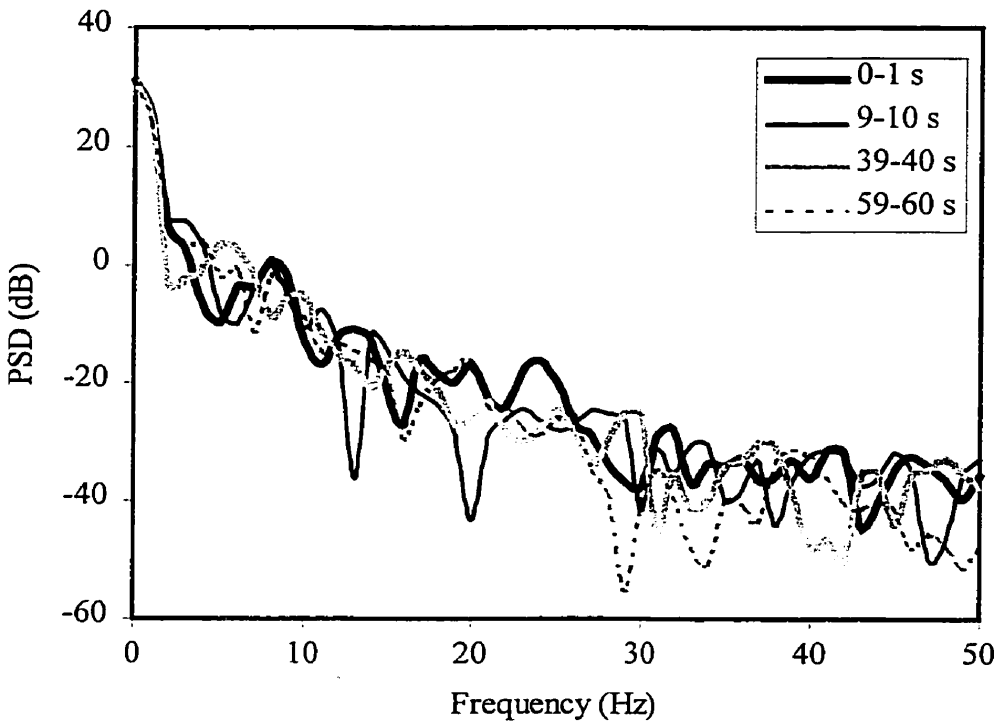

Figure 5.5 Power Spectral Density Function of Different Time Zone for Sand-Water System (1 s calculation period)

Comparing the results of Figures 5.4 and 5.5 shows that the length of the time interval over which the ensemble average PSD function was calculated did not significantly affect the spectrum.

The autocovariance function was also employed in this work, and was also calculated using Matlab. The results are shown in Figure 5.6. As mentioned in chapter 3, the autocovariance function at $\tau = 0$ is the variance of random data. Although the moving standard deviation decreases, there is no regularity for the peak value of the autocovariance. The reason is that the average value increases for these three different cases due to the additional mass of water added in each case.

5.1.2 Mixed Group B Materials

In this experiment, sand of diameter 281 μm was utilized. The static bed height was 30 cm. The superficial gas velocity was 0.25 m/s and total run time was 1 minute. Figure 5.7 shows the pressure fluctuation curve of dry bed. The average pressure during one minute is 4.14 kPa.

1680g of sand was then removed from the bed and replaced with an equal mass of large sized sand of diameter 574 μm so that the total mass in the bed remained constant. The larger sand had the same particle density as smaller sized sand. The larger sand was introduced to simulate the effects of particle agglomeration and bogging. The air flow

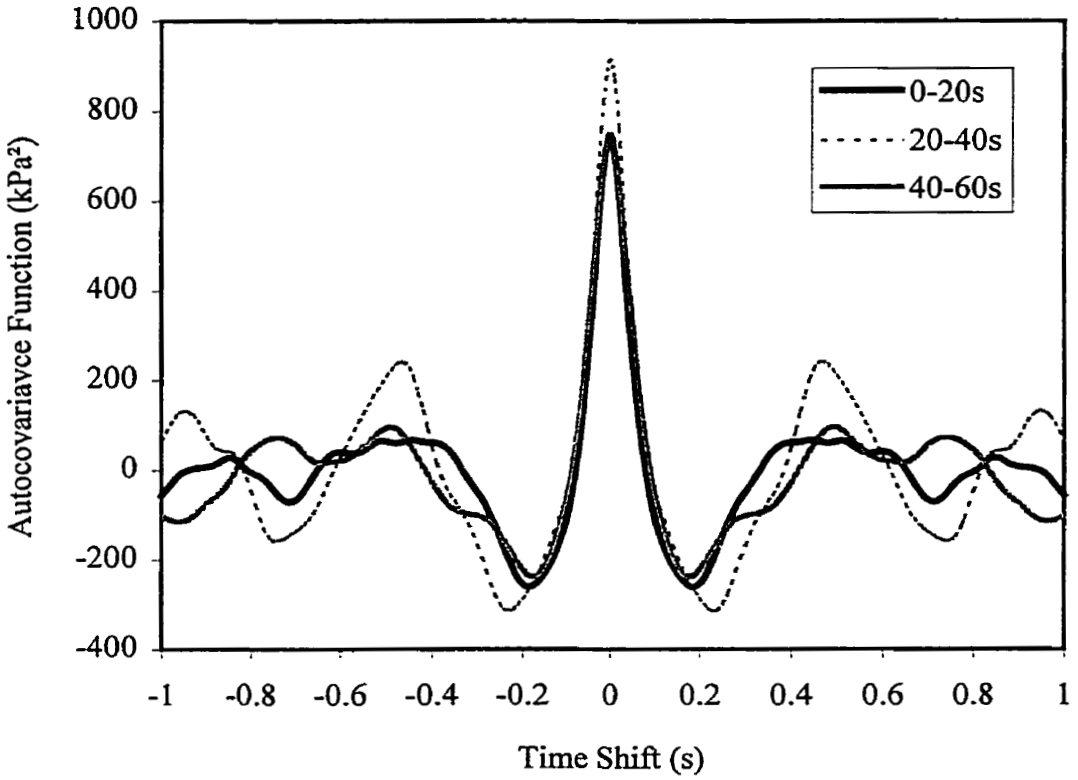

Figure 5.6 Autocovariance Function of Different Time Zone for Sand-Water System

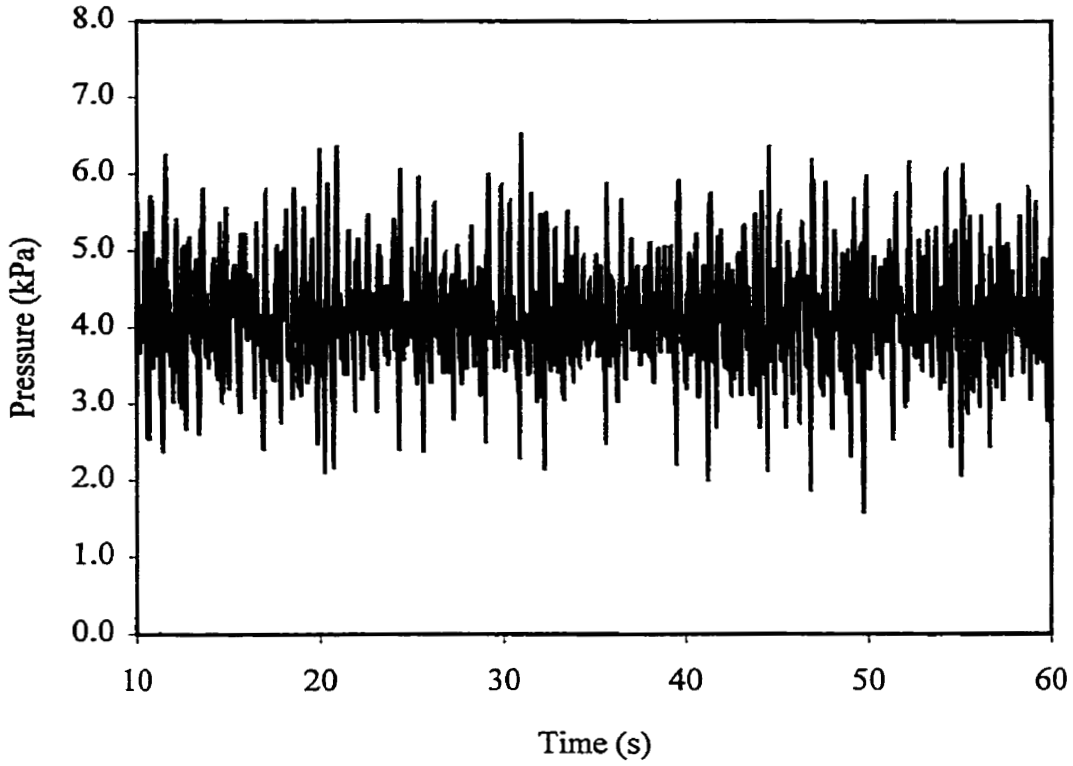

Figure 5.7 Pressure Fluctuation with Time for Smaller Sand

rate and run time were maintained at the values used in the previous experiments. Figure 5.8 shows the pressure fluctuation of the mixed bed. The average pressure of all the points is 4.20 kPa. This shows that the total pressure drop is equal to the total weight in the bed.

In order to check if there is segregation of the mixed sand, sieve analysis was performed. A sample of the mixed sand was taken from the surface of the fluidized bed. Table 5.5 shows the result of the sieve analysis and Figure 5.9 gives the mass fraction curve as a function of the particle diameter. The actual mass ratio of larger sand to smaller sand in the bed was 0.23. From Figure 5.9, the mass fraction of two areas (representing different sand sizes) was 0.82 and 0.18 respectively and the ratio of the mass fractions was 0.22. This indicates that there was no segregation of the sands in the bed. The larger sand was therefore well mixed in the bed and did not deposit on the bottom of the bed.

Figure 5.10 and Figure 5.11 give the standard deviation function of the pressure signals for the small sand and the mixed sand, respectively. The moving standard deviation was calculated in the same manner as the previous experiment. For just small sand, the average standard deviation was 0.655 kPa, and the average standard deviation for mixed sand was 0.586 kPa. This shows general agreement with the experimental results of sand with water. The formation of particle agglomerates leads to an increase in the effective particle diameter and results in a lower standard deviation of the pressure

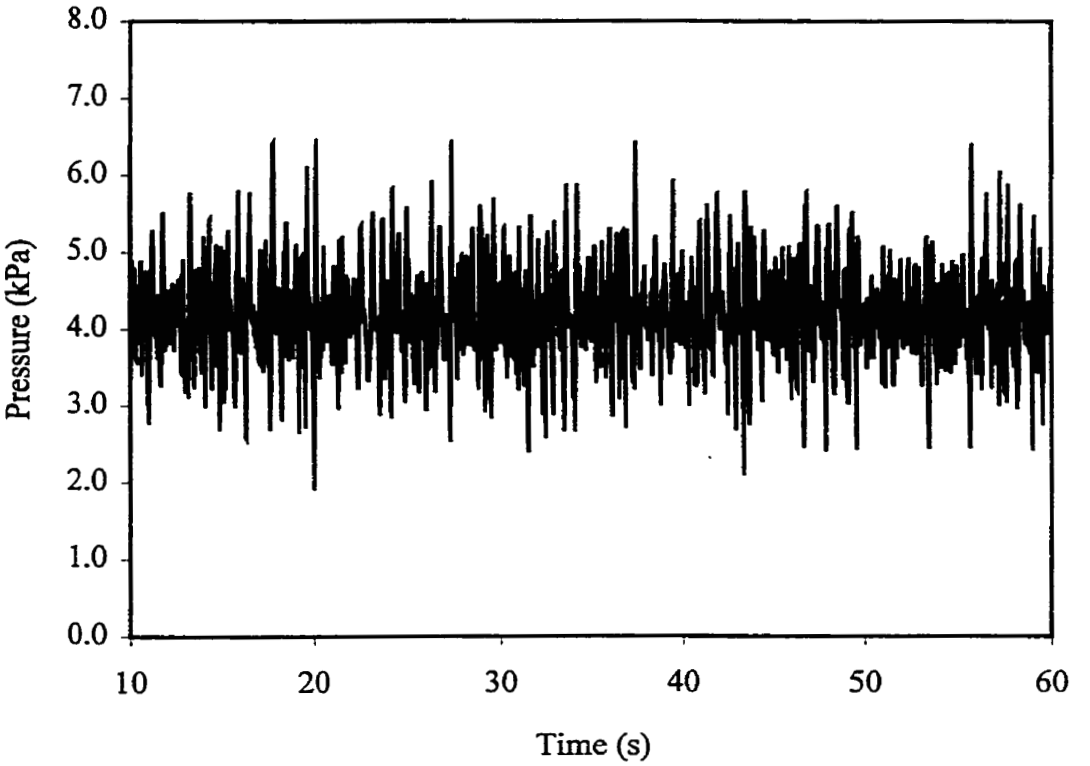

Figure 5.8 Pressure Fluctuation with Time for Mixed Sand

Table 5.5 Sieve Analysis of Mixed Sand

Diameter (μm)		Average dpi(μm)	mass (g) original	with sand (g)	net mass (g)	mass (g)	xi	cumulative xi
<106		106	361.82	361.88	0.06	0.06	1.7563E-04	1.7563E-04
106	125	115.5	363.75	363.82	0.07	0.13	2.0491E-04	3.8054E-04
125	150	137.5	381.12	381.93	0.81	0.94	2.3711E-03	2.7516E-03
150	180	165	391.69	398	6.31	7.25	1.8471E-02	2.1222E-02
180	212	196	369.41	390.81	21.4	28.65	6.2643E-02	8.3865E-02
212	250	231	375.88	411.44	35.56	64.21	1.0409E-01	1.8796E-01
250	300	275	380.69	464.1	83.41	147.62	2.4416E-01	4.3212E-01
300	355	327.5	407.1	518.32	111.22	258.84	3.2557E-01	7.5768E-01
355	425	390	409.77	429.88	20.11	278.95	5.8867E-02	8.1655E-01
425	500	462.5	402.45	422.19	19.74	298.69	5.7784E-02	8.7433E-01
500	710	605	431.66	472.12	40.46	339.15	1.1844E-01	9.9277E-01
710	850	780	452.05	454.35	2.3	341.45	6.7326E-03	9.9950E-01
>850		850	458.24	458.41	0.17	341.62	4.9763E-04	1.0000E+00
				Sum	341.62		1.0000E+00	

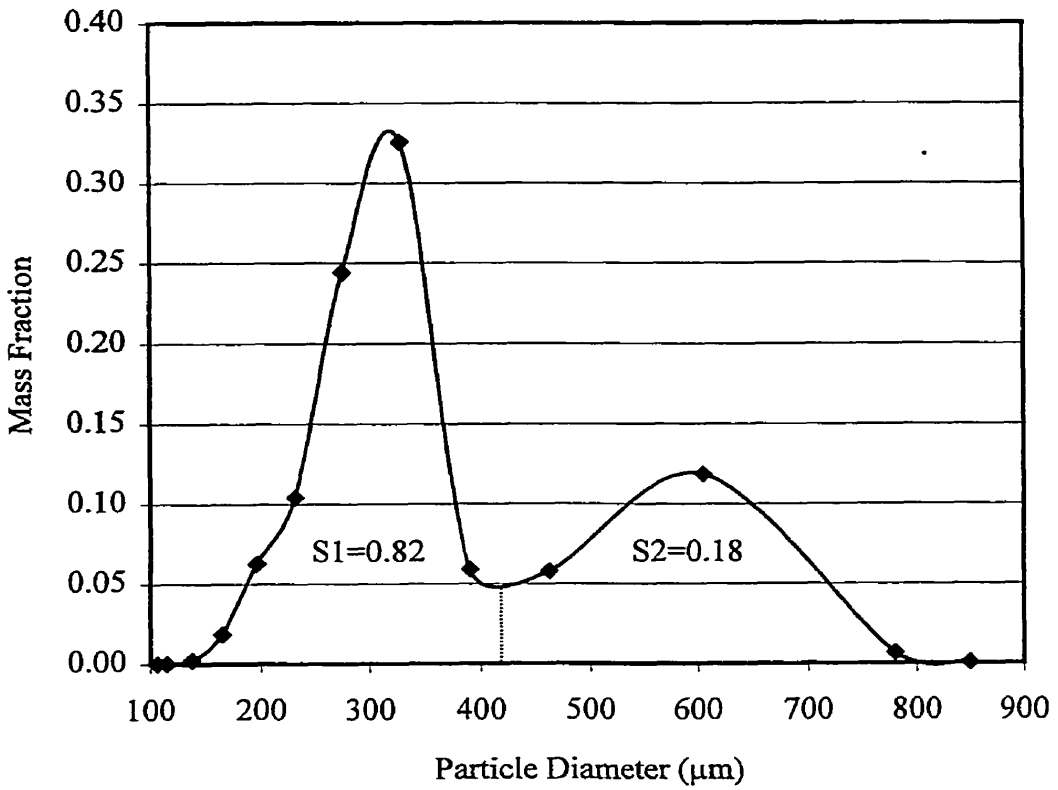

Figure 5.9 Mass Fraction with Particle Diameter for Mixed Sand

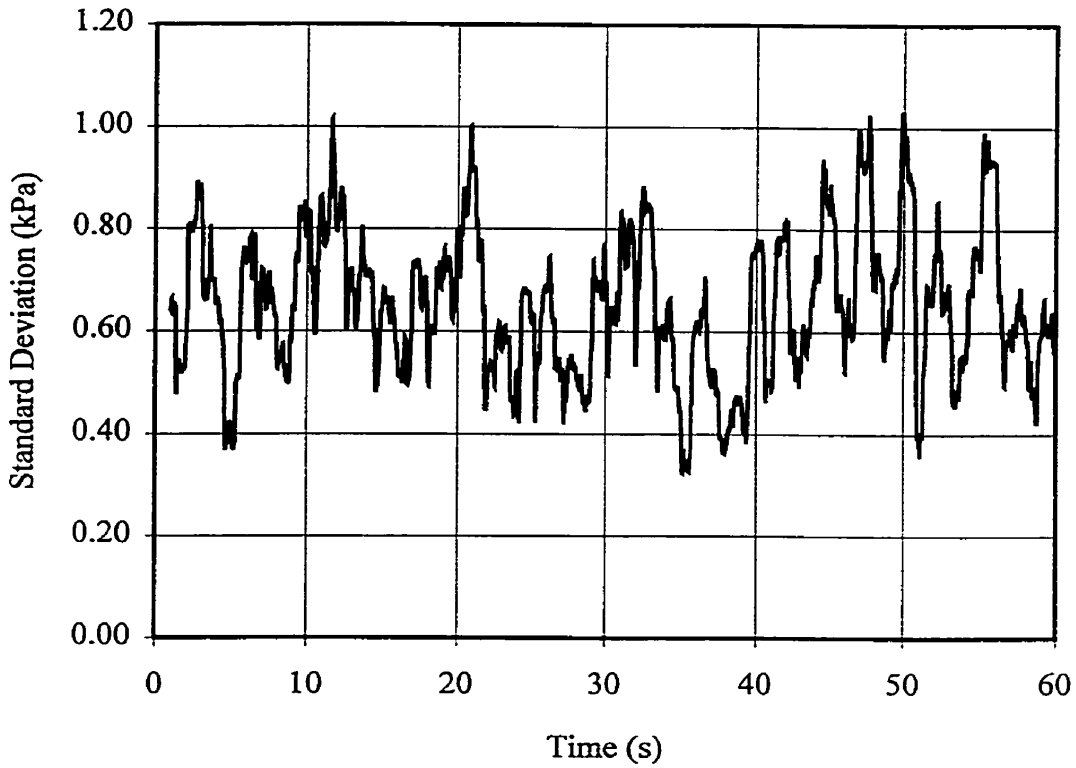

Figure 5.10 Standard Deviation of Pressure with Time for Smaller Sand

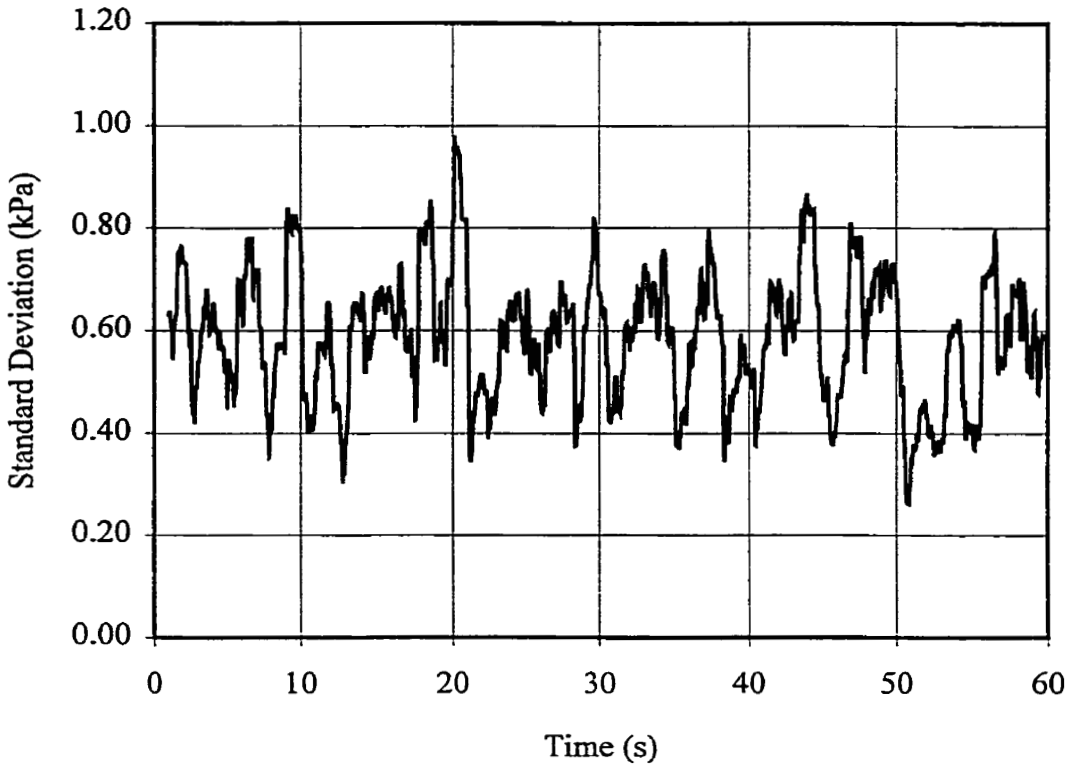

Figure 5.11 Standard Deviation of Pressure with Time for Mixed Sand

signal. Increasing the average particle diameter by the addition of larger sand shows the same effect.

The PSD function curves are shown in Figure 5.12. It is shown that there is no significant difference between the smaller sand and the mixed sand.

Figure 5.13 shows the autocovariance function of pressure signal for the smaller sand and the mixed sand. The peak value of the mixed sand is lower because the average pressures of these two experiments are the same, while the amplitude of the pressure fluctuations of mixed sand is smaller.

5.1.3 Group B Materials (Sand) with Group D Materials (Beads)

The first section of this experiment was the same as that of the previous experiment. A 30cm static bed height of smaller sand was used. The superficial gas velocity was 0.25 m/s and the run time was 60 seconds. Figure 5.14 shows the pressure signal. The average pressure was 4.40 kPa.

Glass beads having a larger diameter but the same particle density were introduced into the bed in order to simulate particle agglomeration. Four experiments were conducted. In each case a mass of sand was removed from the bed equal to that of the bead added in order to maintain the overall mass of the bed constant. The experiments were conducted

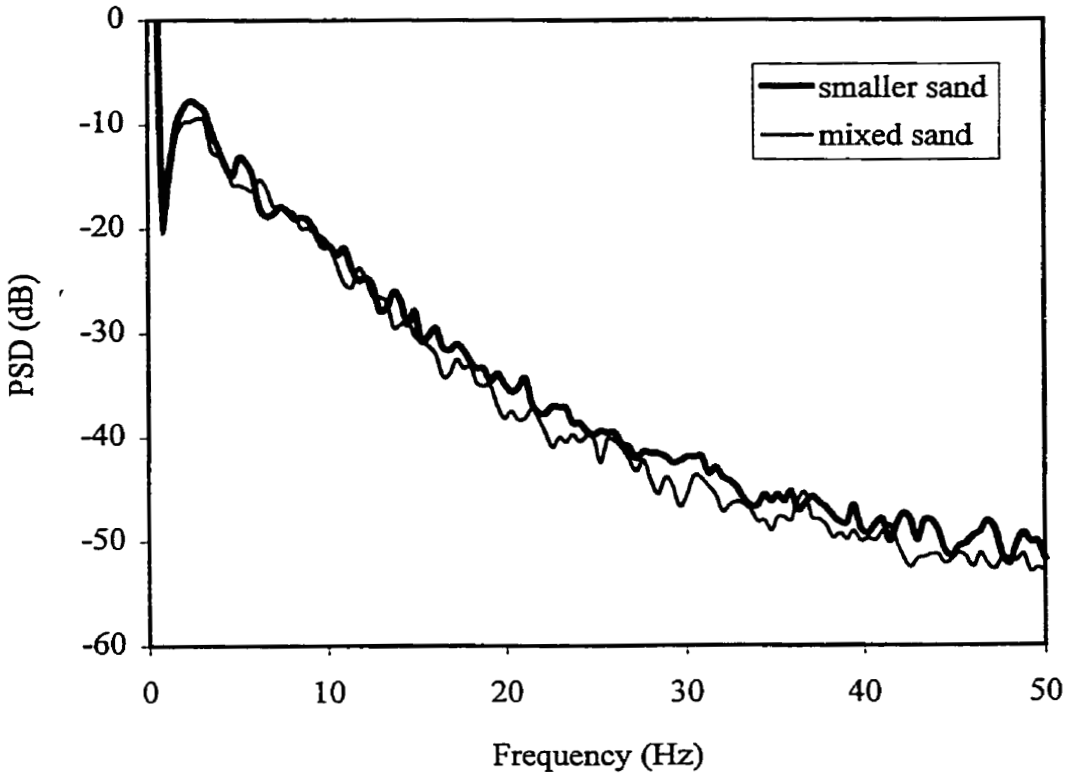

Figure 5.12 Power Spectral Density Function for Smaller Sand and Mixed Sand

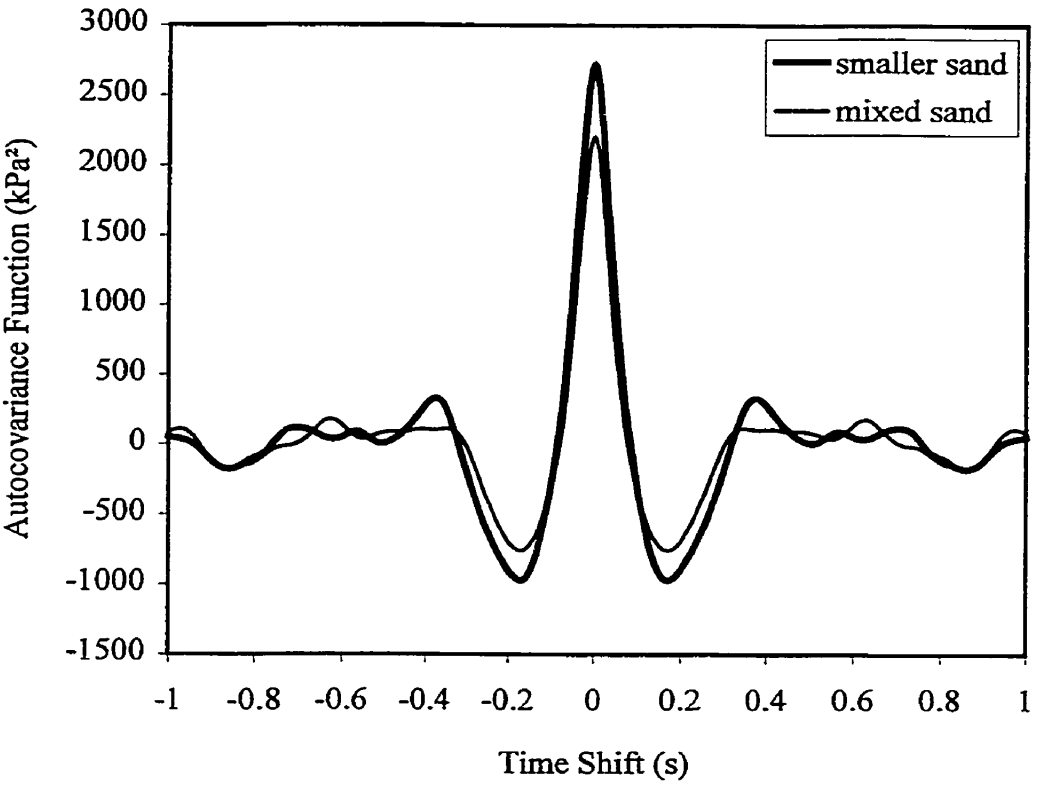

Figure 5.13 Autocovariance Function for Smaller Sand and Mixed Sand

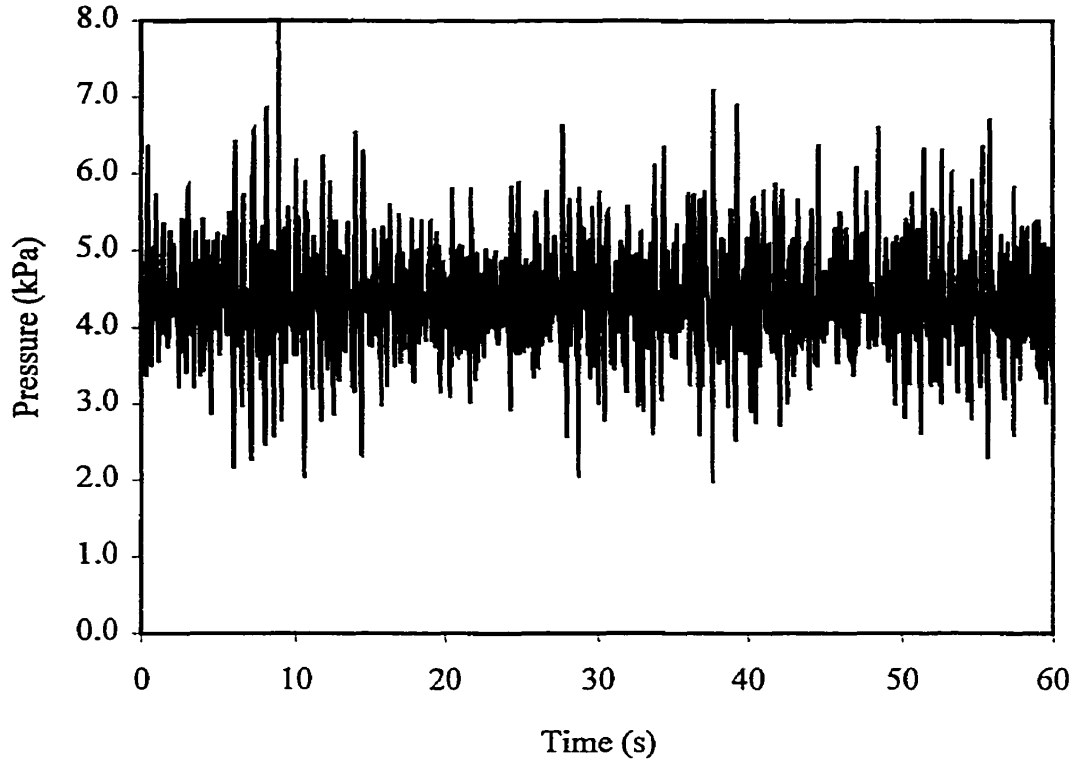

Figure 5.14 Pressure Fluctuation with Time (Smaller Sand)

with glass bead additions of 193 g, 810 g, 1217 g and 1777 g beads respectively. Figures 5.15-5.18 show the pressure fluctuation data for these four experiments. The average value of each curve was 4.40 kPa, 3.93 kPa, 3.79 kPa and 3.31 kPa respectively. During the experiments, the glass beads were observed to settle at the bottom of the bed. From above pressure data, it also shows that the beads deposited on the bottom of the bed are supported by the distributor resulting in an overall reduction in the bed pressure drop.

Figures 5.19-5.23 show the moving standard deviation function for different beads concentrations. The average values were 0.65 kPa, 0.59 kPa, 0.56 kPa, 0.56 kPa and 0.45 kPa respectively. It is clear that the standard deviation decreases as more and more beads were added.

The PSD function curves are shown in Figure 5.24. It is shown there is no significant difference between smaller sand and sand with different concentrations of glass beads.

Figure 5.25 shows the autocovariance function of the smaller sized sand and the sand-bead. The peak value decreases continuously with increasing bead concentration.

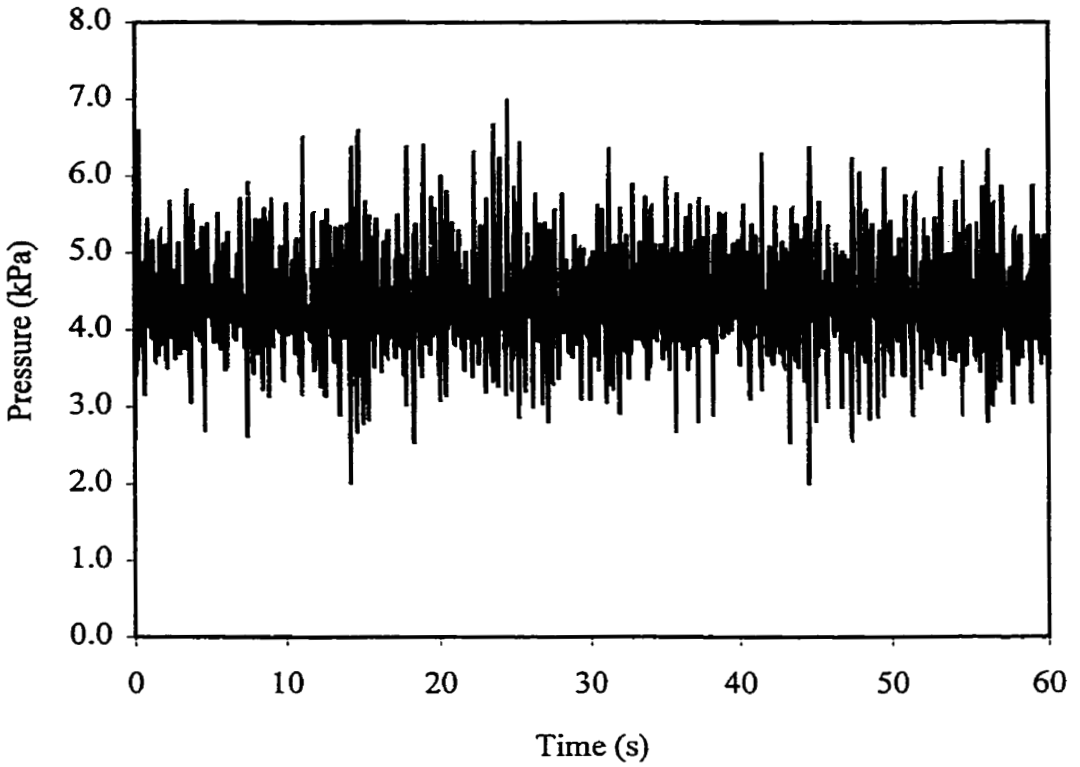

Figure 5.15 Pressure Fluctuation with Time (Smaller Sand with 19·3g Beads)

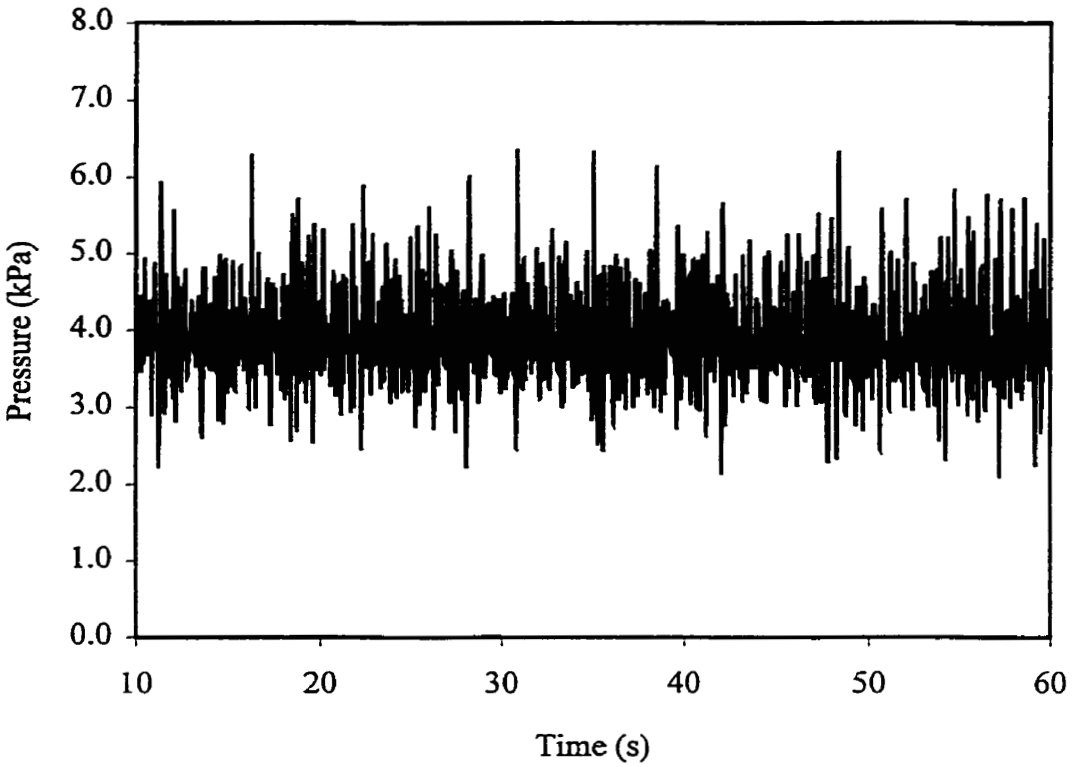

Figure 5.16 Pressure Fluctuation with Time (Smaller Sand with 810g Beads)

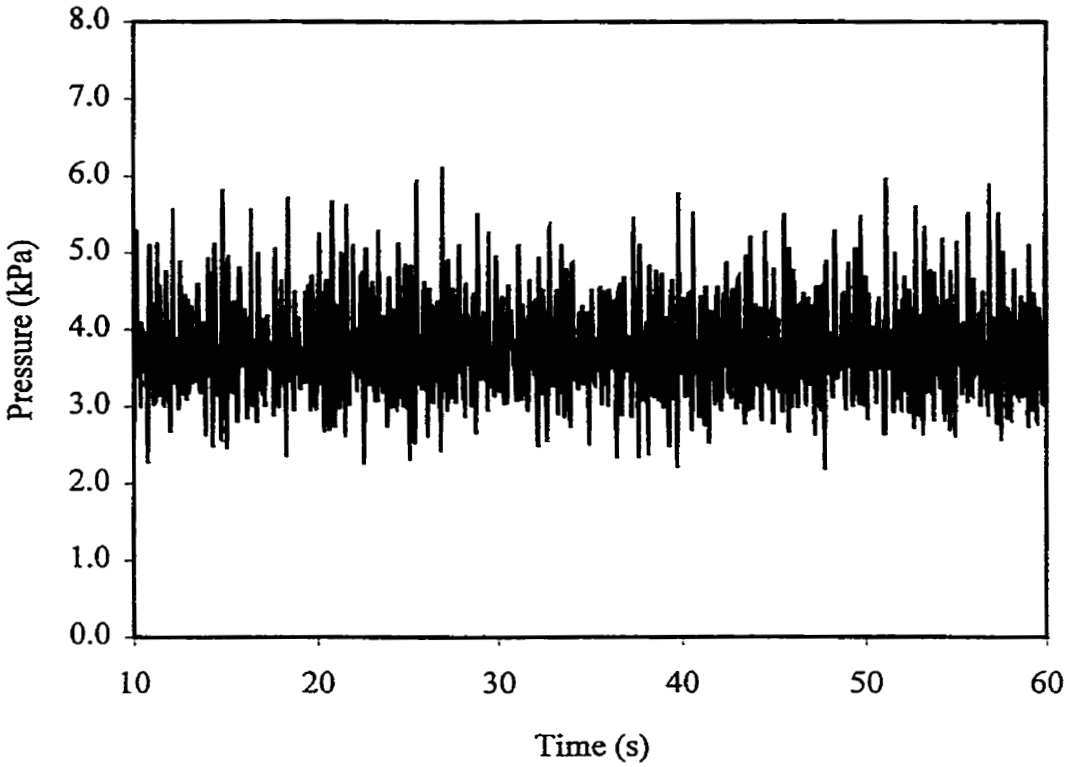

Figure 5.17 Pressure Fluctuation with Time (Smaller Sand with 1217g Beads)

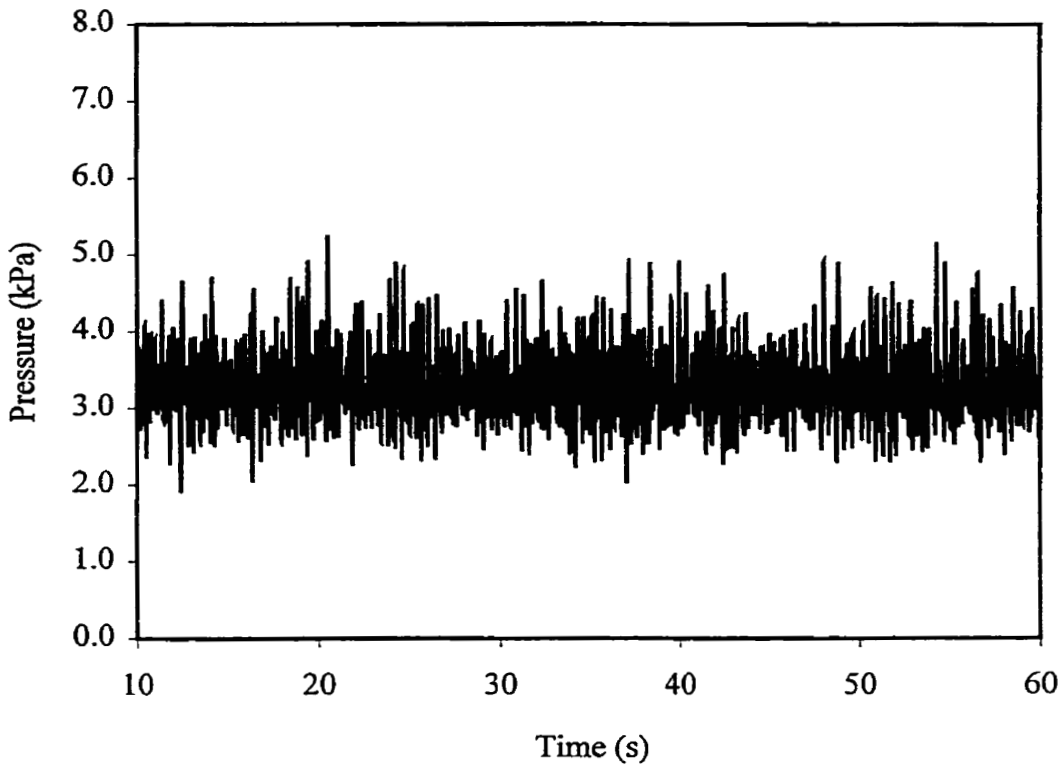

Figure 5.18 Pressure Fluctuation with Time (Smaller Sand with 1777g Beads)

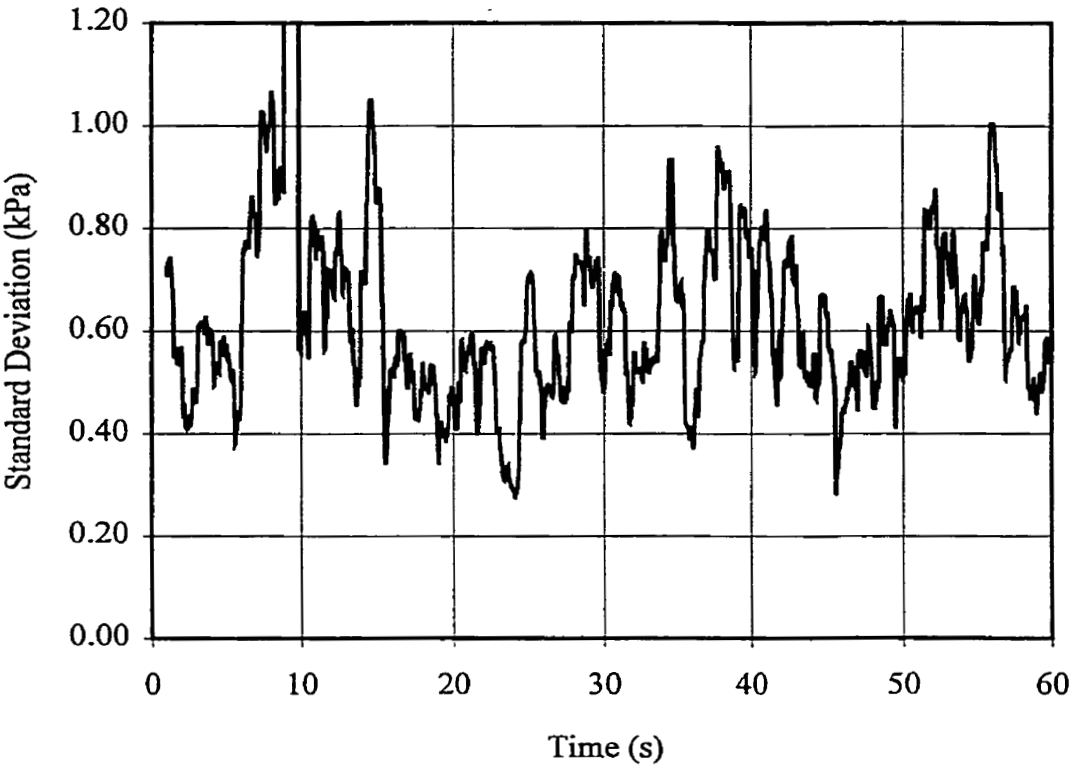

Figure 5.19 Standard Deviation with Time (Smaller Sand)

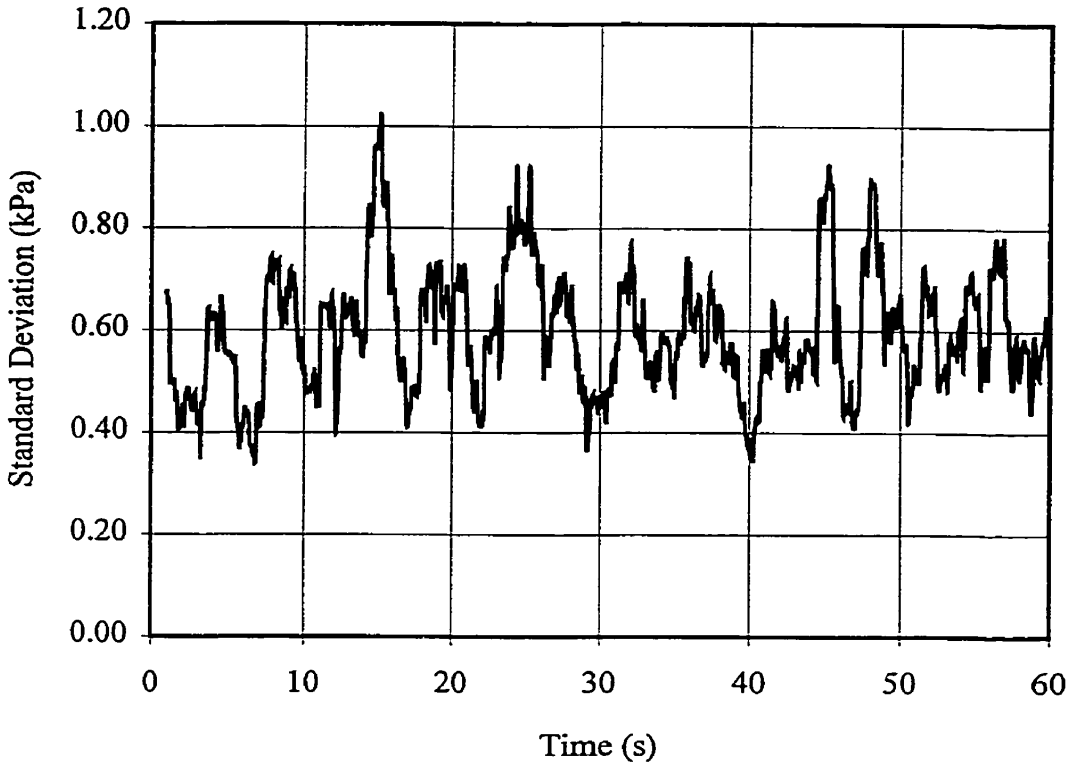

Figure 5.20 Standard Deviation with Time (Smaller Sand with 193g Beads)

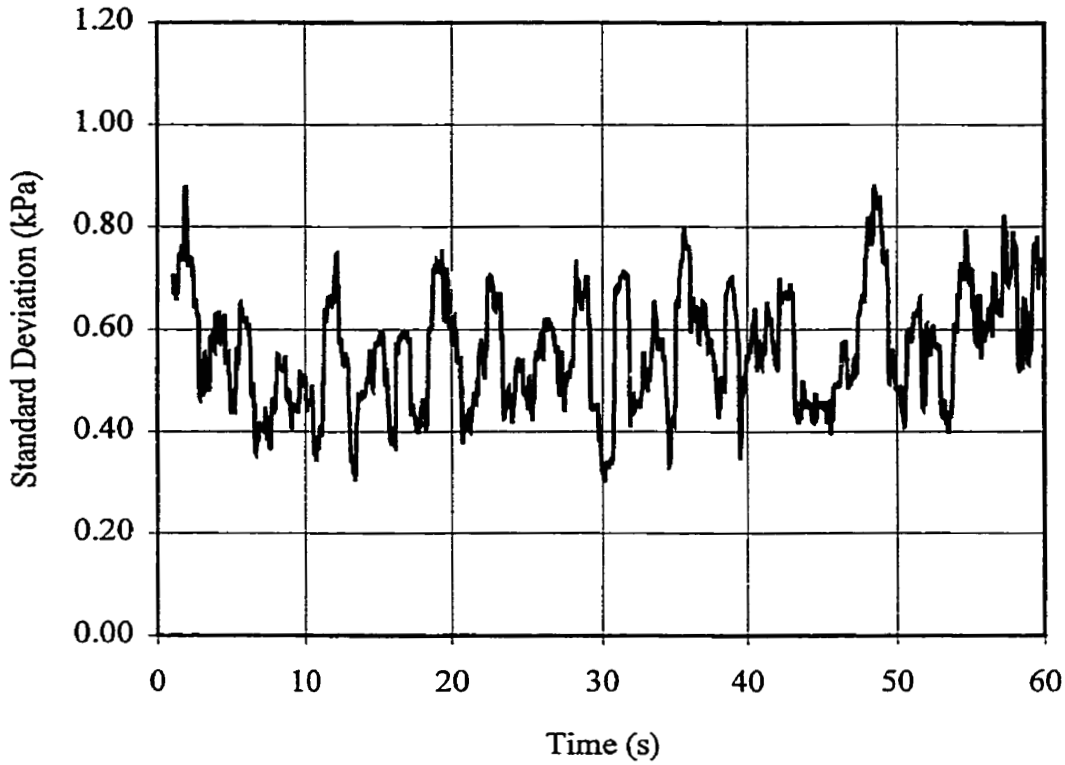

Figure 5.21 Standard Deviation with Time (Smaller Sand with 810g Beads)

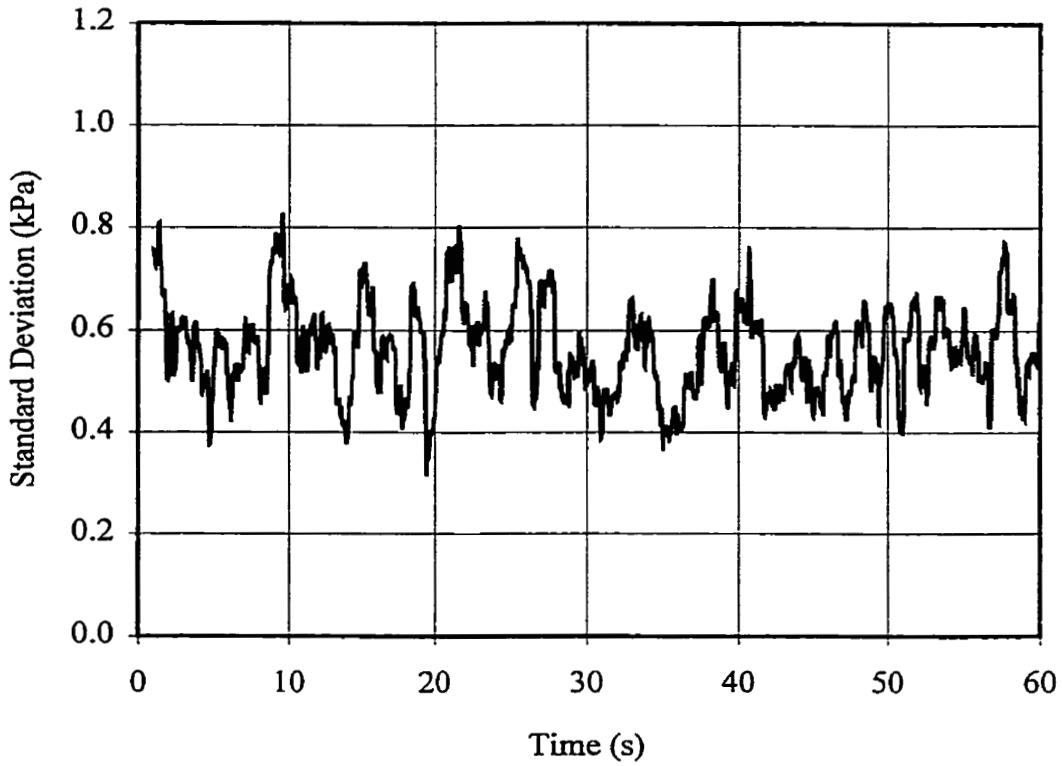

Figure 5.22 Standard Deviation with Time (Smaller Sand with 1217g Beads)

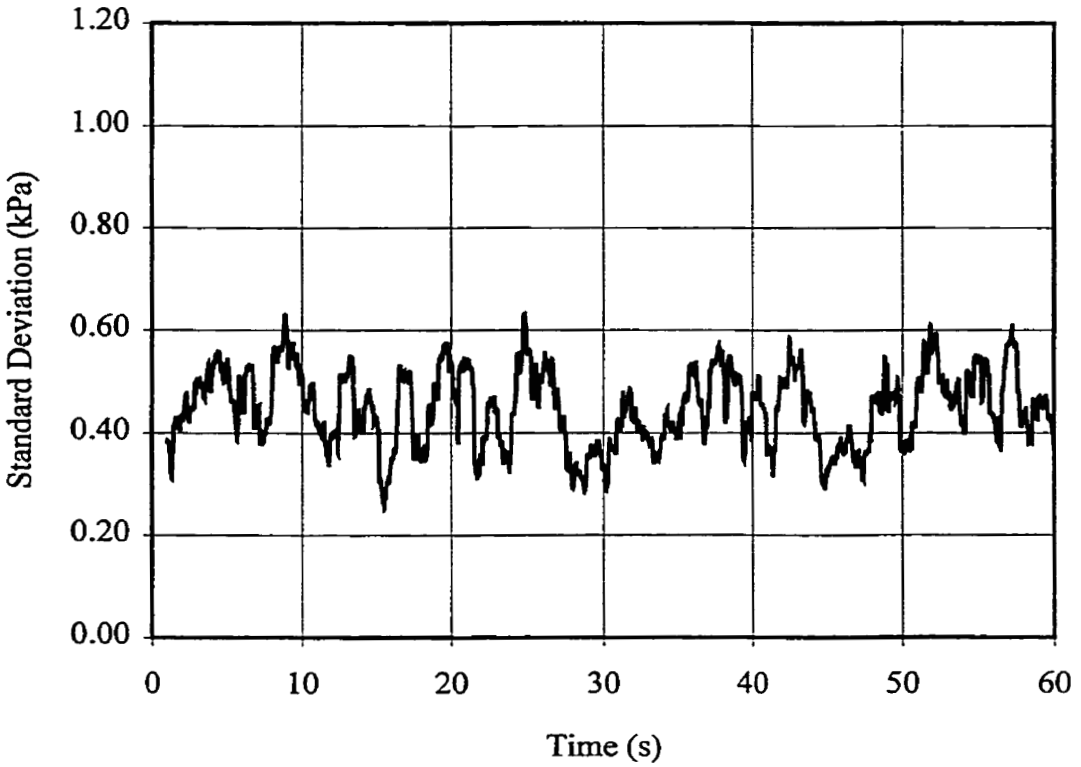

Figure 5.23 Standard Deviation with Time (Smaller Sand with 1777g Beads)

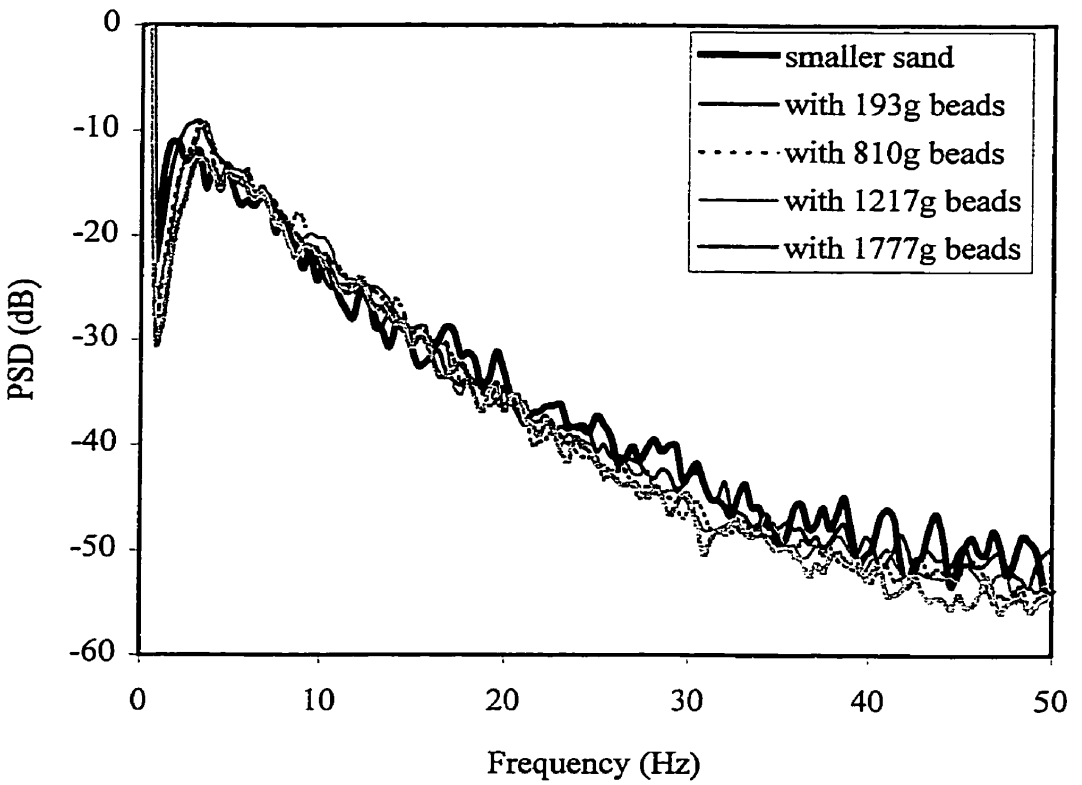

Figure 5.24 Power Spectral Density Function for Different Beads Concentration

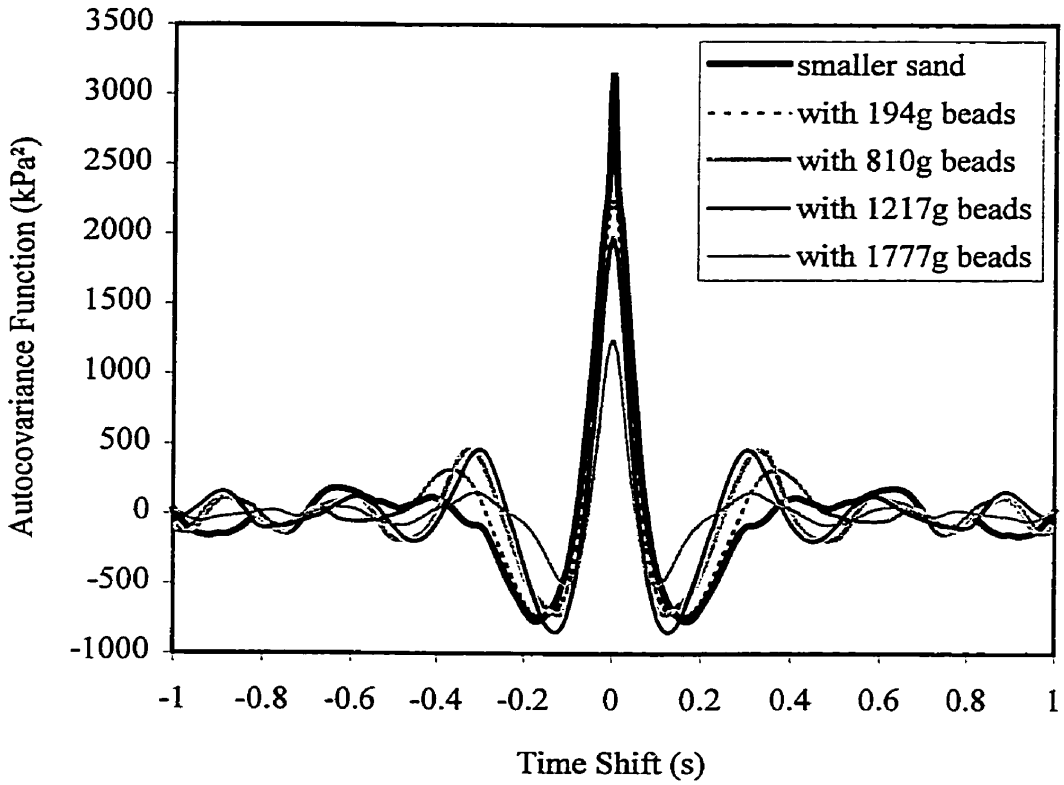

Figure 5.25 Autocovariance Function for Different Beads Concentration

5.1.4 Conclusions for Group B Materials

For mixed sand and sand with different concentration beads, the average particle diameters were calculated according to Equation 3.1. and tabulated in Table 5.6 along with the standard deviation of the pressure signal for each average diameter. The scatter points in Figure 5.26 show the data and the straight line was a best-fit line for these points. It is clear that the standard deviation decreases linearly with increasing particle diameter.

To summarize the conclusions for Group B materials:

1. Moving standard deviation function is a good indication of particle agglomeration.
2. Power spectral density function is not a useful method to detect bogging.
3. Autocovariance function can detect bogging if the total weight in the bed remains constant.

5.2 Defluidization of Group A Materials (FCC)

Two experiments were performed in this section; one with FCC agglomerated with water, the other with FCC and polystyrene beads. Polystyrene was used to simulate particle agglomerates in a similar manner to the experiments of the previous section.

Table 5.6 Standard Deviation with Different Average Particle Diameter

	Average Particle Diameter (μm)	Standard Deviation (kPa)
Smaller Sand	281	0.6536
With 193g beads	287	0.5943
With 810g beads	308	0.5599
With 1680g larger sand	312	0.5888
With 1217g beads	321	0.5619
With 1777g beads	348	0.4489

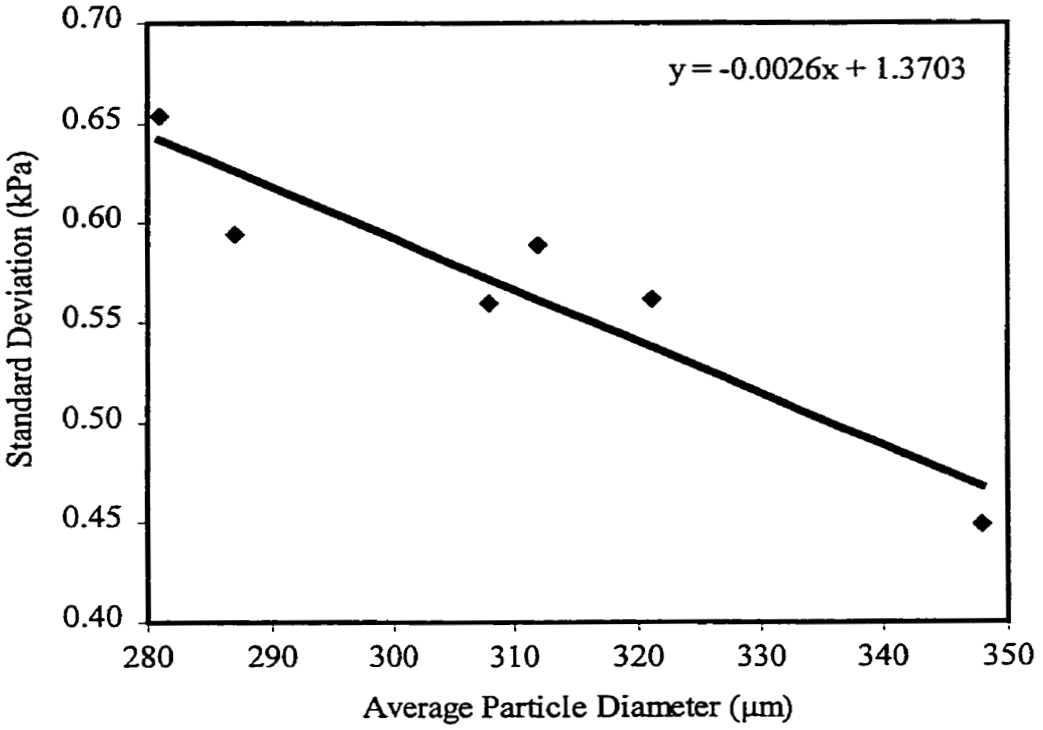

Figure 5.26 Standard Deviation with Different Particle Diameter

5.2.1 Group A (FCC) Materials with Water

30cm static bed height of FCC was used with a superficial gas velocity of 0.07 m/s. For the first 20 seconds of operation no water was introduced. After 20 seconds, 4 g/s of water was sprayed into the bed. The total run time was 200 seconds. Figure 5.27 shows the pressure fluctuation data and Figure 5.28 shows the moving average pressure value with time. The behavior is very similar to that observed with sand and water. Before 20 seconds, the pressure fluctuates normally. Between 20s-185s, the pressure increases due to the mass of water added.

As shown in Table 5.7, the observed pressure increase is again approximately equal to the water mass sprayed into the bed. After 185s, the pressure decreases due to bogging. Visual observation indicated the appearance of channels after about 100 seconds operation, far before the onset of drop in the bed pressure at 185s. Therefore, the drop in bed pressure cannot be used to detect bogging.

Figure 5.29 gives the standard deviation function of the pressure signal, and show standard deviation to be approximately constant. No substantial change in the standard deviation before and after bed agglomeration is indicated. Although the bed pressure drop decreased after bogging as shown in Figure 5.27, the amplitude of the pressure fluctuation remained about the same. Therefore, the standard deviation cannot detect bogging for FCC.

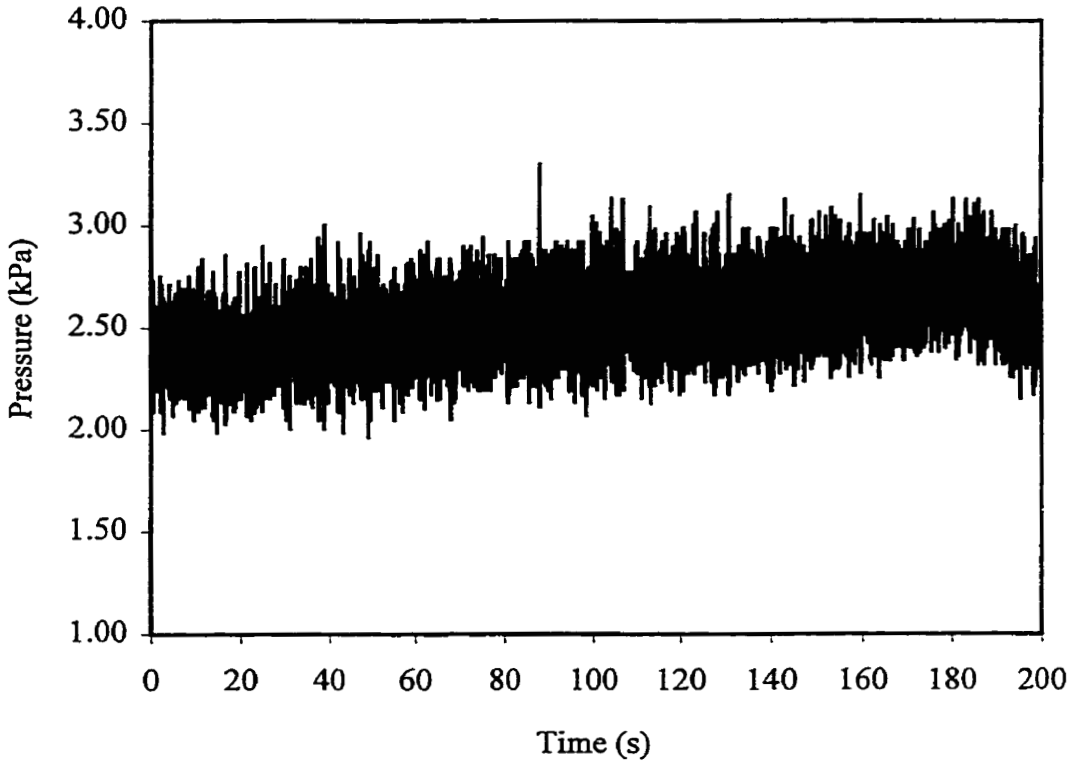

Figure 5.27 Pressure Fluctuation with Time for FCC-Water System

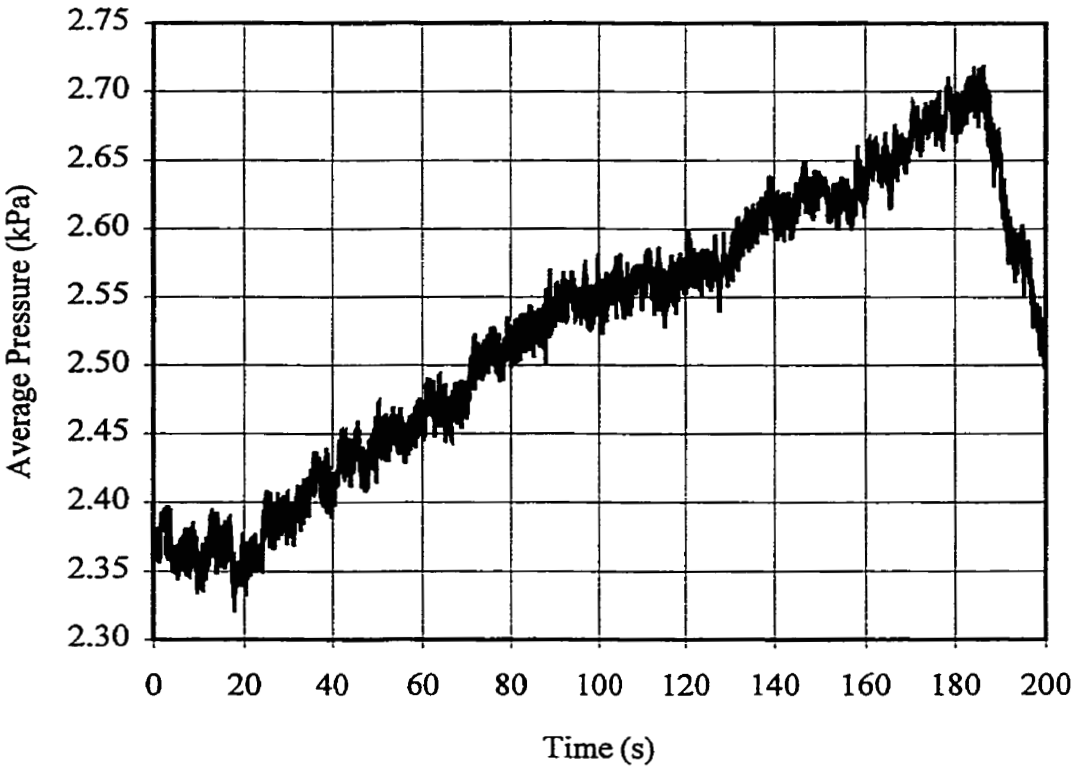

Figure 5.28 Average Pressure with Time for FCC-Water System

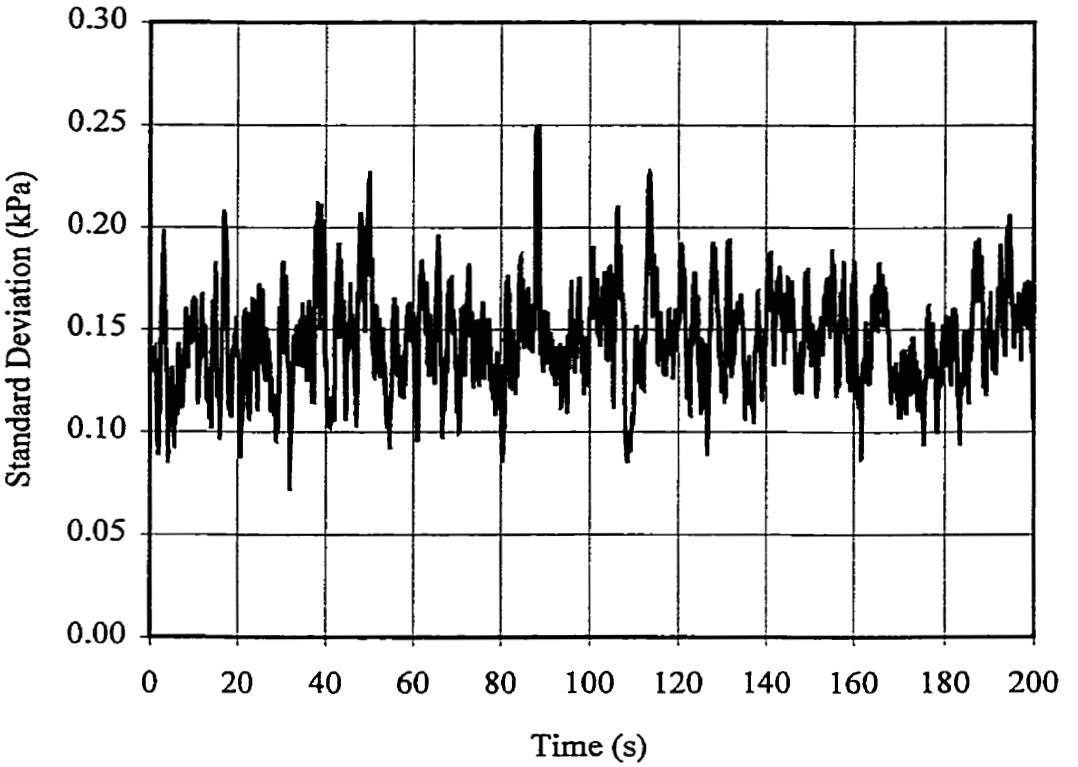

Figure 5.29 Standard Deviation of Pressure with Time for FCC-Water System

Table 5.7 Water Balance for FCC-Water System

Water sprayed between 20-180 s, g	640
Total water weight G = mg, N	6.27
Average Pressure at 20 s, kPa	2.34
Average Pressure at 180 s, kPa	2.70
Pressure increase between 20-180 s, kPa	0.36
F = P×A (bed cross section area), N	6.22

Figure 5.30 and Figure 5.31 give the PSD and autocovariance function of the pressure fluctuation. Similar behavior is observed to that for the sand-water system. No apparent change in the PSD and autocovariance function occurred.

5.2.2 Group A (FCC) Materials with Group B (Polystyrene) Materials

In this set of experiments a 30cm static bed height of FCC was used with a superficial gas velocity of 0.04 m/s. The pressure signal was recorded for 1 minute. The results are shown in Figure 5.32. The average value of pressure was 2.41 kPa.

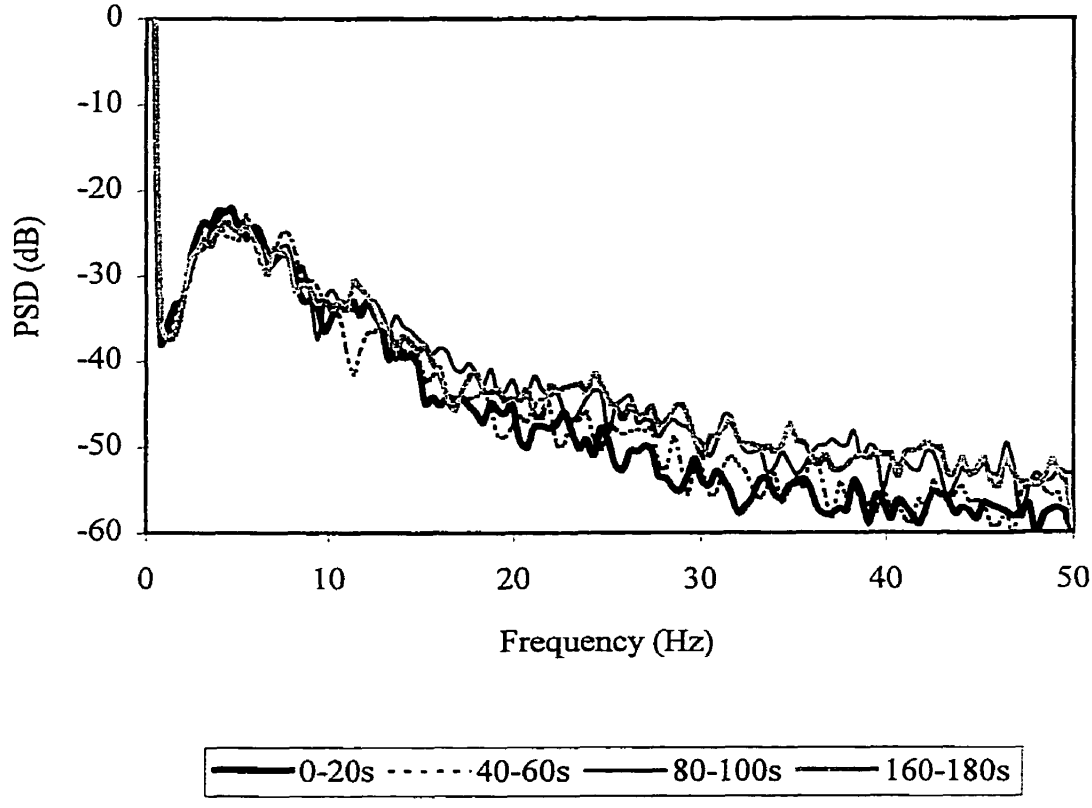

Figure 5.30 Power Spectral Density Function of Different Time Zone for FCC-Water System

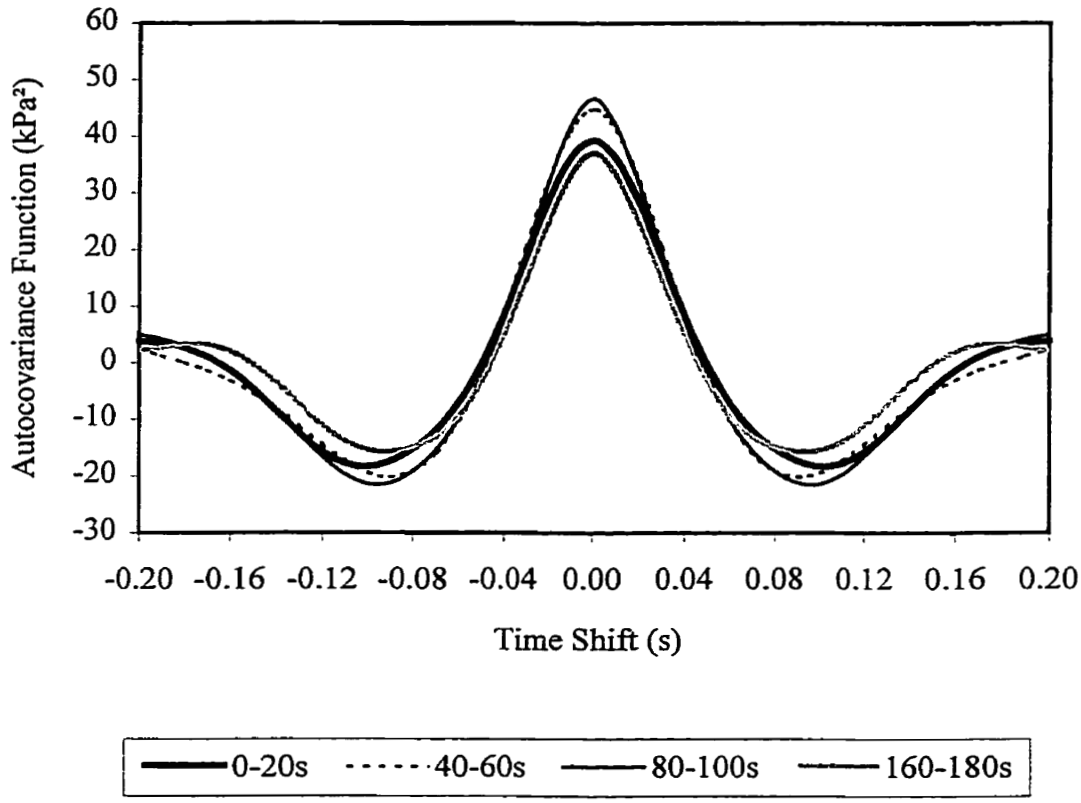

Figure 5.31 Autocovariance Function of Different Time Zone for FCC-Water System

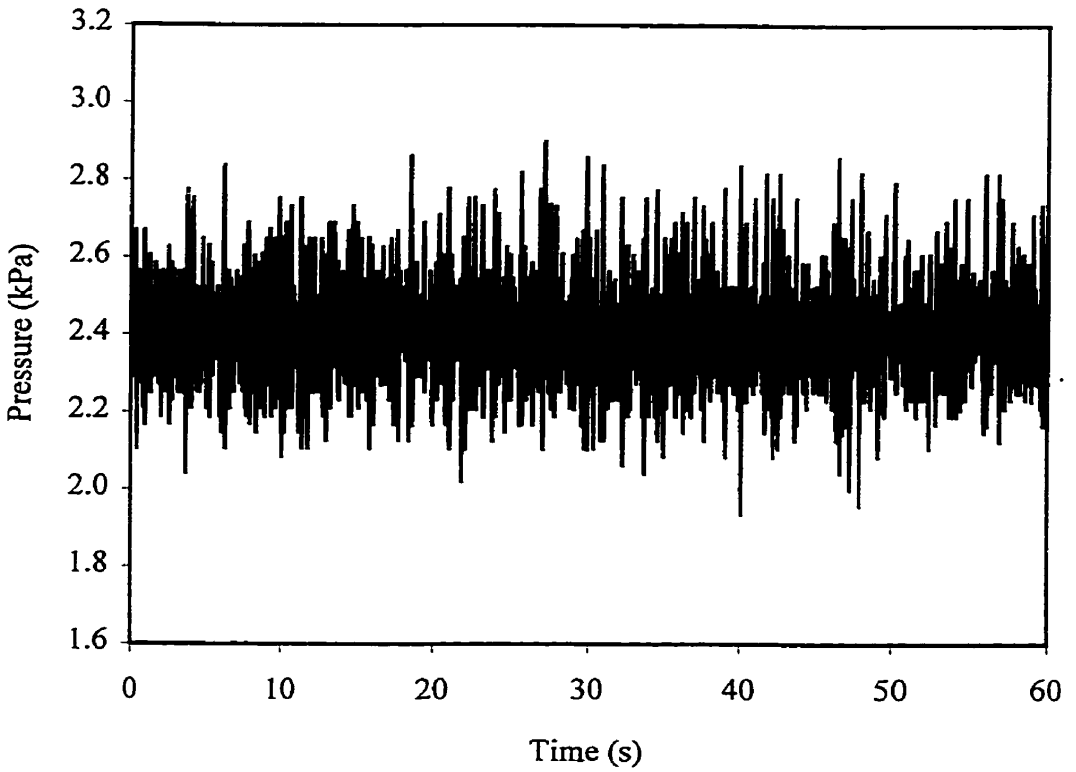

Figure 5.32 Pressure Fluctuation with Time for FCC

906g of FCC was then removed from the bed and replaced with an equal mass of polystyrene particles, keeping the total mass in the bed constant. Figure 5.33 shows the pressure data for the mixed particle system. The average value of pressure is 2.40 kPa, approximately the same value as for the experiment without polystyrene. After the experiment, a sample was taken from the surface of the fluidized particles. The FCC and polystyrene were separated using a sieve and weighted separately. The mass ratio of two types of particles was equal to the ratio of total mass of particles in the bed indicating that the bed was well mixed. Unlike the experiments with sand and glass beads, no particle segregation was observed and no particles were deposited on the distributor.

Figure 5.34 and Figure 5.35 show the standard deviation function of the two experiments. The average value of the standard deviation was 0.13 kPa and 0.11 kPa, respectively. As before, the larger average particle diameter results in a lower standard deviation.

The PSD function curves are shown in Figure 5.36. Again, there is no discernable difference between FCC and FCC with polystyrene.

Figure 5.37 shows the autocovariance function of FCC and FCC with polystyrene. The peak value of FCC with polystyrene decreased because the amplitude decreased while the average pressure remained constant.

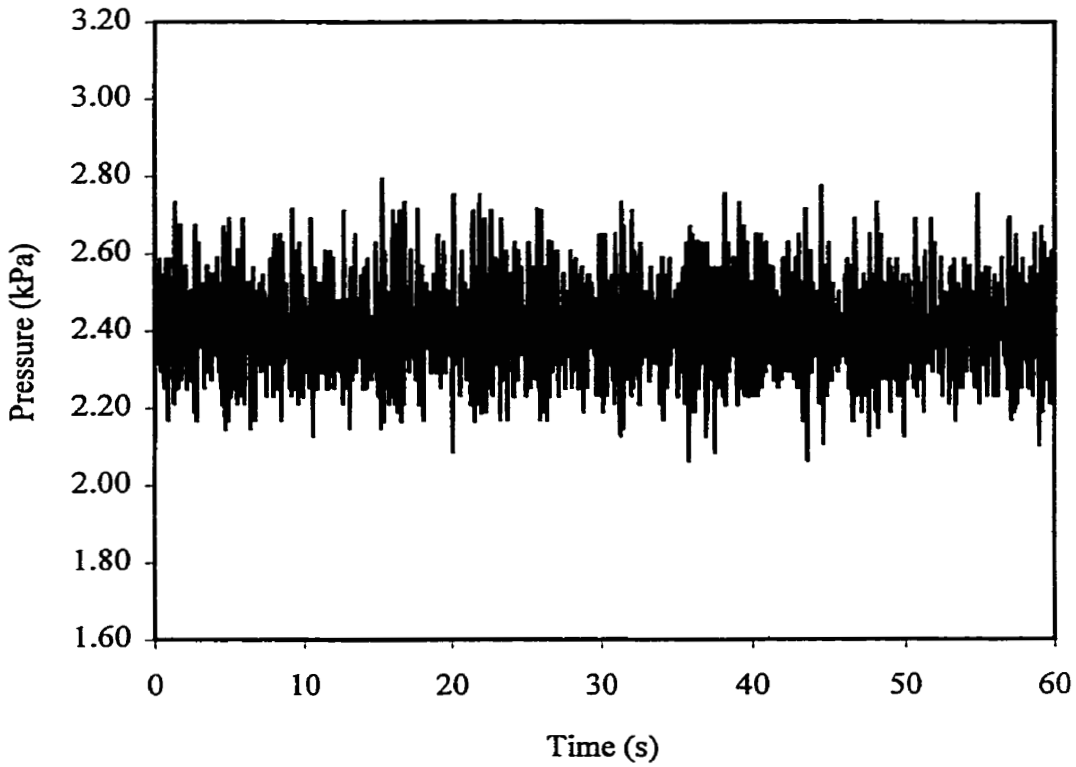

Figure 5.33 Pressure Fluctuation with Time (FCC with Polystyrene)

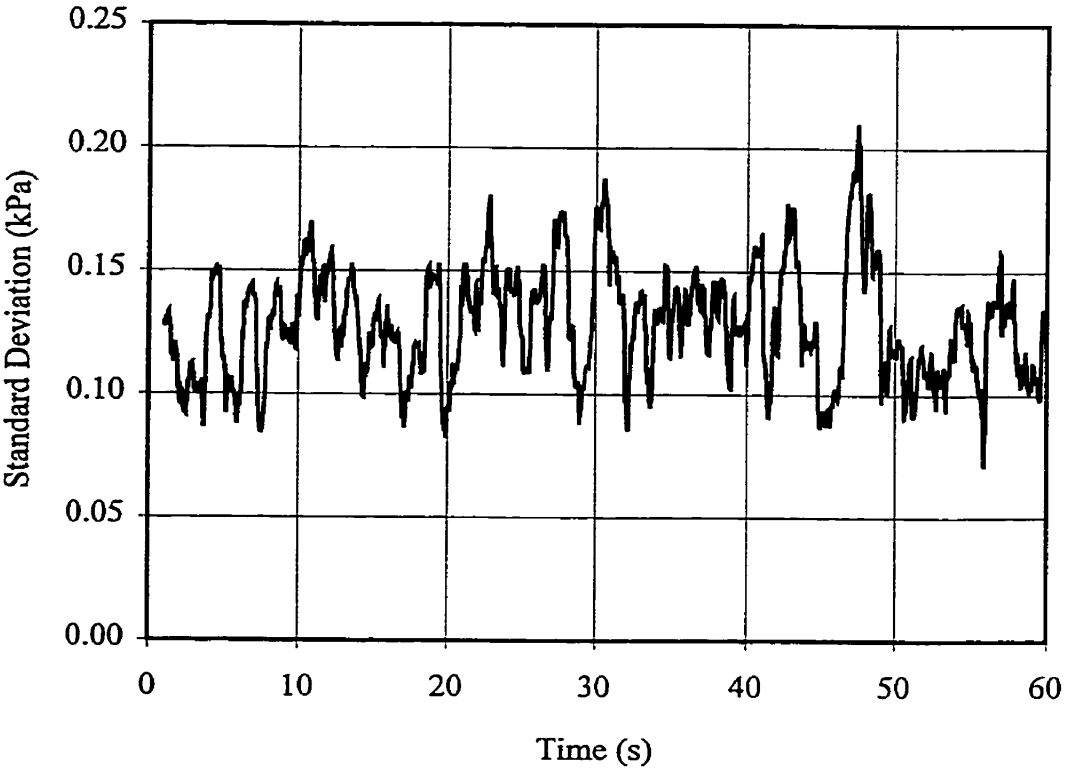

Figure 5.34 Standard Deviation with Time for FCC

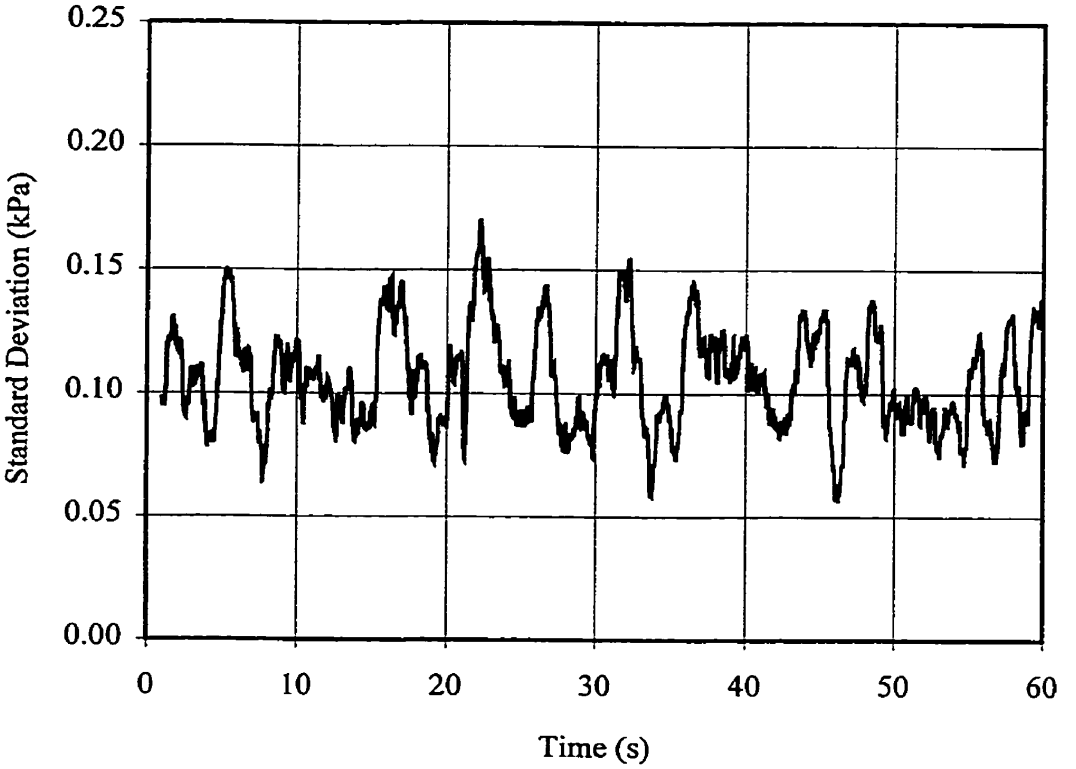

Figure 5.35 Standard Deviation with Time (FCC with Polystyrene)

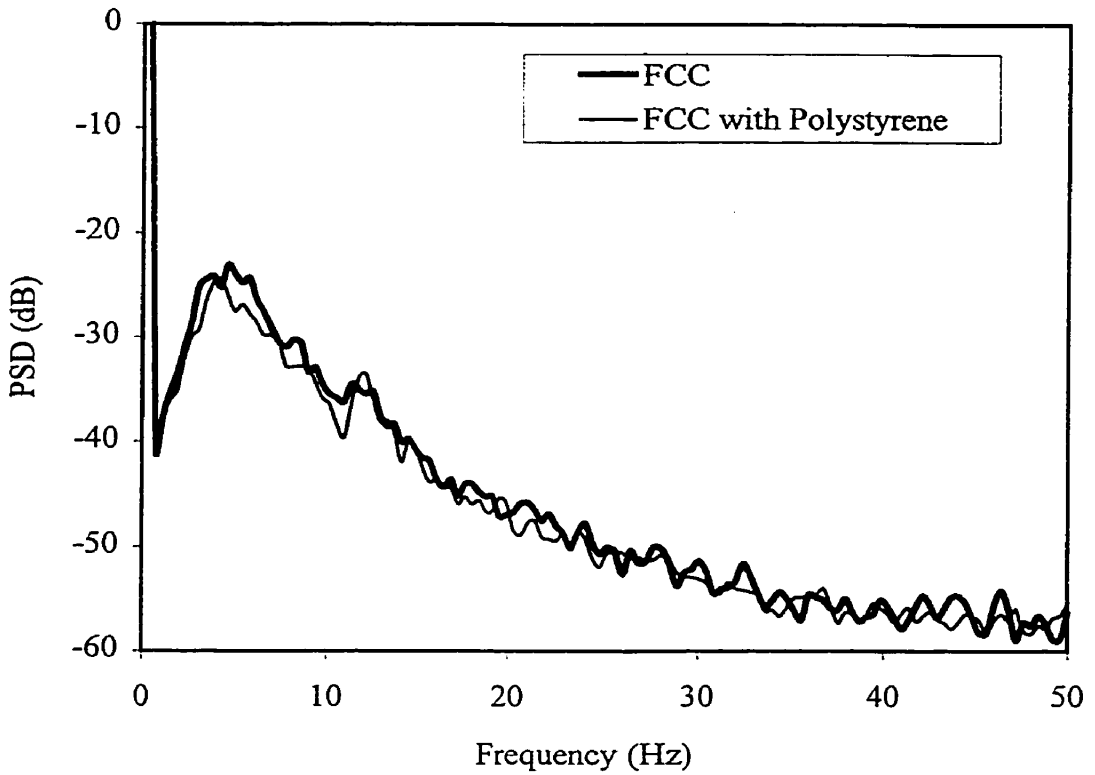

Figure 5.36 Power Spectral Density Function with Time
(FCC and FCC with Polystyrene)

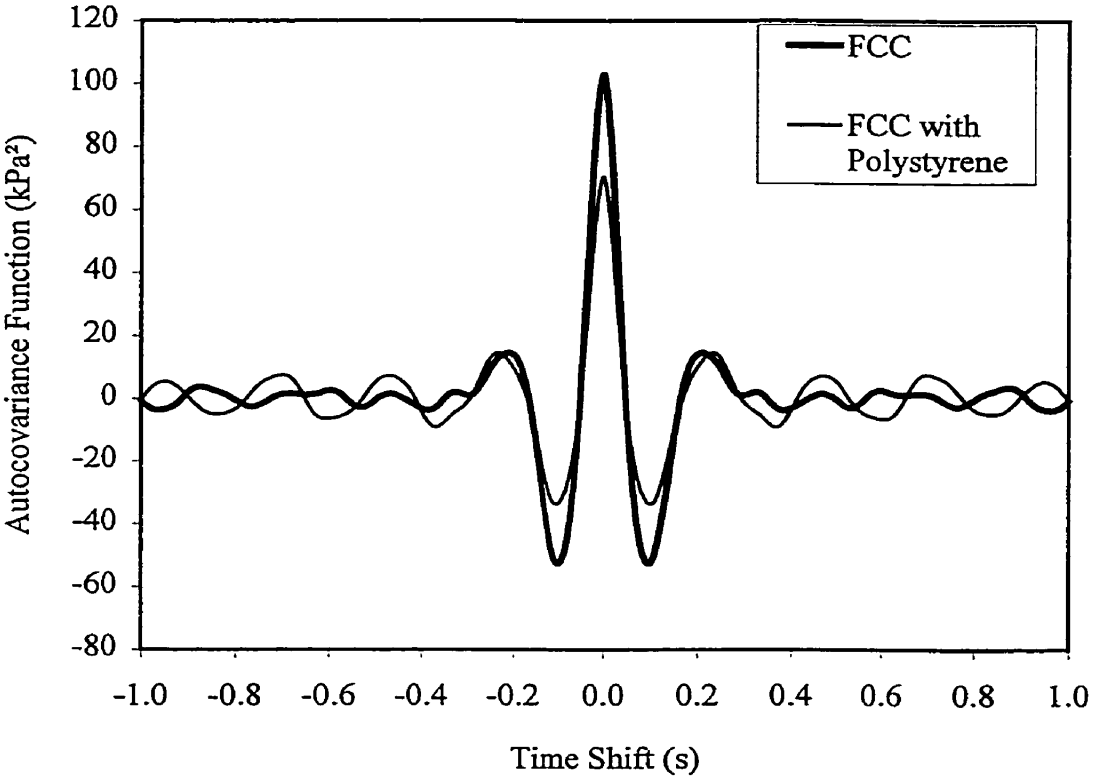

Figure 5.37 Autocovariance Function with Time
(FCC and FCC with Polystyrene)

5.2.3 Conclusions for Group A Materials

When the water was sprayed onto FCC, it was supposed that most water was absorbed into particles because FCC is very porous, and highly absorbant. Addition of water to the bed does not result in particle stickiness, and particle agglomerates do not form. The average particle diameter remains constant, although the increased particle density changed the minimum fluidization velocity. However, the effect was not as dramatic as the increase in effective particle diameter due to the formation of particle agglomerates in the sand-water system. When a small amount of FCC was wetted, channels appeared and the bed pressure drop decreased. The remaining dry FCC still fluidized resulting in constant pressure fluctuation amplitude.

In the experiment with FCC and polystyrene, polystyrene was used to simulate FCC aggregates, and the standard deviation of the mixed particles decreased compared with that of FCC alone. It is conjectured that if group A particles are non-porous, the standard deviation will also decrease due to bogging.

To summarize the conclusions for the Group A material:

1. If particles are very porous, no method was found to detect bogging.

2. Standard deviation and autocovariance functions may provide an indication of bogging for FCC in the presence of agglomerates.
3. The power spectral density function is not a useful method to detect bogging.

Chapter 6

Conclusions and Recommendations

6.1 Conclusions

The experiments conducted in this study indicated that the standard deviation of the pressure signal decreases with increasing particle diameter. As mentioned in chapter 3, the two-phase theory of fluidization would indicate that when particle diameter increases, the minimum fluidization velocity will increase, and both the bubble size and rise velocity will decrease. As the bubble size decreases the amplitude of pressure fluctuation would be expected to decrease, consistent with observation.

When water is sprayed onto sand, the water will coat the surface of sand, resulting in the formation of particle agglomerates. The effective diameter of the particle increases, and the standard deviation of the pressure fluctuation decreases.

When the water was sprayed onto FCC, it was assumed that most of the water was absorbed into the porous FCC particles. Particle agglomeration is therefore negated and the effective particles diameter is unchanged. Although the particle density due to the absorbance of water can change the minimum fluidization velocity, the two-phase theory would predict that the effect would be smaller than that due to changes in the particle diameter. When a small amount of FCC was wetted, channels appeared and the pressure

drop across the bed decreases. The unwetted FCC remained fluidized and the pressure fluctuation amplitude remained constant.

In the experiment with FCC and polystyrene, polystyrene was used to simulate the formation of FCC aggregated. The standard deviation of the mixed particles decreased compared with that of FCC alone. It is therefore conjectured that if group A particles are non-porous, the standard deviation will also decreases due to bogging.

The following summarizes the conclusions of this work.

1) For sand, the moving standard deviation function is an effective method to detect bogging. The autocovariance function can detect particle agglomeration if the total mass in the bed stays constant.
2) For FCC, no method was found to detect the onset of bogging. Additional research should be conducted to examine the bogging behavior of these materials.
3) The power spectral density function is not a useful method to detect bogging.

6.2 Recommendations

Further work is required to elucidate the agglomerative behavior of FCC in the presence of water. It is also recommended that future studies should be on laboratory scale fluid

coking units to examine the agglomerative behavior of the fluid coke-bitumen systems to confirm that the standard deviation of the pressure signal may be used to detect the onset of bogging. This information would be required to implement a control system to detect the bogging in an industrial fluid coking unit.

References

Basu, P., "A Study of Agglomeration of Coal-Ash in Fluidized Beds", Can. J. Chem. Eng., **60**, December (1982).

Bendat, J.S., "Principles and Applications of Random Noise Theory", John Wiley and Sons, Inc., New York (1977).

Bendt, J.S. and A.G. Piersol, "Engineering Applications of Correlation and Spectral Analysis", Second Edition, John Wiley and Sons, Inc., New York (1993).

Bi, H.T. and J.R. Grace, "Effect of Measurement Method on the Velocities Used to Demarcate the Onset of Turbulent Fluidization", The Chemical Engineering Journal, **57**, 261-271 (1995).

Brown, R.G. and J.W. Nilsson, "Introduction to Linear Systems Analysis", John Wiley and Sons, Inc., New York (1962).

Busch, R.A., " Fluid Coking: Seasoned Process Takes on New Jobs", Oil Gas J., **68,** (14), 102-111 (1970).

Cai, P., S.P. Chen, Y. Jin, Z.Q. Yu, and Z.W. Wang, "Effect of Operating Temperature and Pressure on the Transition from Bubbling to Turbulent Fluidization", AIChE Symposium Series, **85,** (270), 37-43 (1985).

Crandall, S.H. and W.D. Mark, "Random Vibrations in Mechanical Systems", Academic Press, New York (1963).

Davenport, J.B. and W.R. Root, "An Introduction to the Theory of Random Signals and Noise", McGraw-Hill Book Co., Inc., New York (1958).

Davidson, J.F. and D. Harrison, "Fluidization Particles", Cambridge University Press, NY (1963).

Ergun, S., Chem. Eng. Prog., **48**, 89 (1952).

Fan, L.T., T.C. Ho, S. Hiraoka and W.P. Walawender, "Pressure Fluctuations in a Fluidized Bed", AIChE J., **27**, 388-396 (1981).

Fan, L.S., S. Satija and K. Wisecarver, "Pressure Fluctuation Measurements and Flow Regime Transitions in Gas-liquid-solid Fluidized Beds", AIChE J., **32**, 338-340 (1986).

Fiocco, R.J., Sc.D. Thesis, Stevens Institute of Technology, Hoboken, N. J. (1964).

Gluckman, M.J., J. Yerushalmi and A.M. Squires, "Defluidization Characteristics of Sticky Agglomerating Bed", Fluidization Technology, **2**, Ed. D.L. Keairns, 395-422, Washington D.C., Hemisphere Publishing Corp. (1976).

Goldenberger, W.M., "Collection of Fly Ash in a Self Agglomerating Fluidized Bed Coal Burner" ASME Meeting, November, Pittsburgh (1967).

Haider A. and O. levenspiel, Powder Technology, **58**, 63 (1989).

Harada, K., "Graduation with Simultaneous Coating and Agglomeration in a Fluidized Bed: Particle Size Distribution and Growth Rate in the Steady State", Kagoku Kogaku, **36**, 79 (1972).

Jakher, R.K., "Hydrodynamics and Mass Transfer in Different Zones in a Three-Phase Fluidized Bed", M.Sc. Thesis, University of Calgary (1998).

Kapur, P.C., "Balling and Graduation", Advances in Chemical Engineering, **10**, Academic Press, New York, 55 (1978).

Kett, T.K., G.C. Lahn and W.L. Schuette, "Flexicoking: A Versatile Residuum Conversation Process", AIChE 67th Annual Meeting, December 2, (1974).

Kunii, D. and O. Levenspiel, "Fluidization Engineering", Second Edition, Butterworth-Heinemann, (1991).

Langston, B.G. and F.M. Stephens, " Self Agglomerating Fluidized Bed Reduction", Journal of Meatal, 312 April (1960).

Lee, Y.W., "Statistical Theory of Communication", John Wiley and Sons, Inc., New York (1960).

Liang, R. and H. Littman, "Statistical Study of the Pressure Fluctuations in a Fluidized Bed", AIChE Symp. Ser., **67,** (116), 11 (1971).

Liss, B., T.R. Blake, A.M. Squires and R. Bryson, "Incipient Defluidization of Sinterable Solids", Fourth International Conference on Fluidization, Japan, June (1983).

Pugsley, T.S., "The Hydrodynamics of Circulating Fluidized Beds", Ph.D. Thesis (1995).

Pulvermacher, B. and E. Ruckenstein, "Two kinds of Self-Preserving Size Spectra of a Cloud of Particles", AIChE J., **21**, 128 (1975).

Satija S. and L.S. Fan, "Characteristics of Slugging Regime and Transition to Turbulent Regime for Fluidized Beds of Large Coarse Particles", AIChE J., **31**, 1554-1562 (1985).

Shuster, W.W. and P. Kisliak, " The Measurement of Fluidization Quality", Chem. Eng. Prog., **48**, 455 (1952).

Sigell, J.H., "Defluidization Phenomena in Fluidized Beds of Sticky Particles at High Temperatures", Ph.D. thesis, City University of New York (1976).

Sigell, J.H., "High-Temperature Defluidization", Powder Tech., **38**, 13 (1984).

Sterns, S.D., "Digital Signal Analysis", Hayden Book Co., Rochelle Park, NJ 223-239 (1975).

Sutherland, K.S., Argonne National Laboratory Report ANL-6907 (1964).

Swinehart, F.M., "A Statistical Study of Local Wall pressure Fluctuations in Gas Fluidized Columns", Ph.D. Dissertation, University of Michigan (1966).

Tardos, G. I., D. Mazzone and R. Pfeffer, "Measurement of Surface Viscosities Using a Dilatometer", Can. J. Chem. Eng., **62**, December (1984).

Tardos, G.I., D. Mazzone and R. Pfeffer, "Destabilization of Fluidized Beds due to Agglomeration, Part I: Theoretical Model", Can. J. Chem. Eng., **63**, June (1985).

Tardos, G.I., D. Mazzone and R. Pfeffer, "Destabilization of Fluidized Beds due to Agglomeration, Part II: Experimental Verification", Can. J. Chem. Eng., **63**, June (1985).

Toomey R.D. and H.F. Johnstone, Chem. Eng. Prog., **48,** 220 (1952).

Werther, J., German Chem. Eng., **1**, 166 (1978).

Werther, J., " Fluidization IV", 93, Engineering Foundation, NY (1983).

Werther, J. and K. Hilligardt, Proc. 3rd World Cong. Of Chem. Eng., Tokyo (1986).

Winkler, German Patent (1922).

Winter, O., "Density and Pressure Fluctuations in Gas Fluidized Beds", AIChE J., **14**, 426 (1968).

Appendix A

Rotameter Calibration

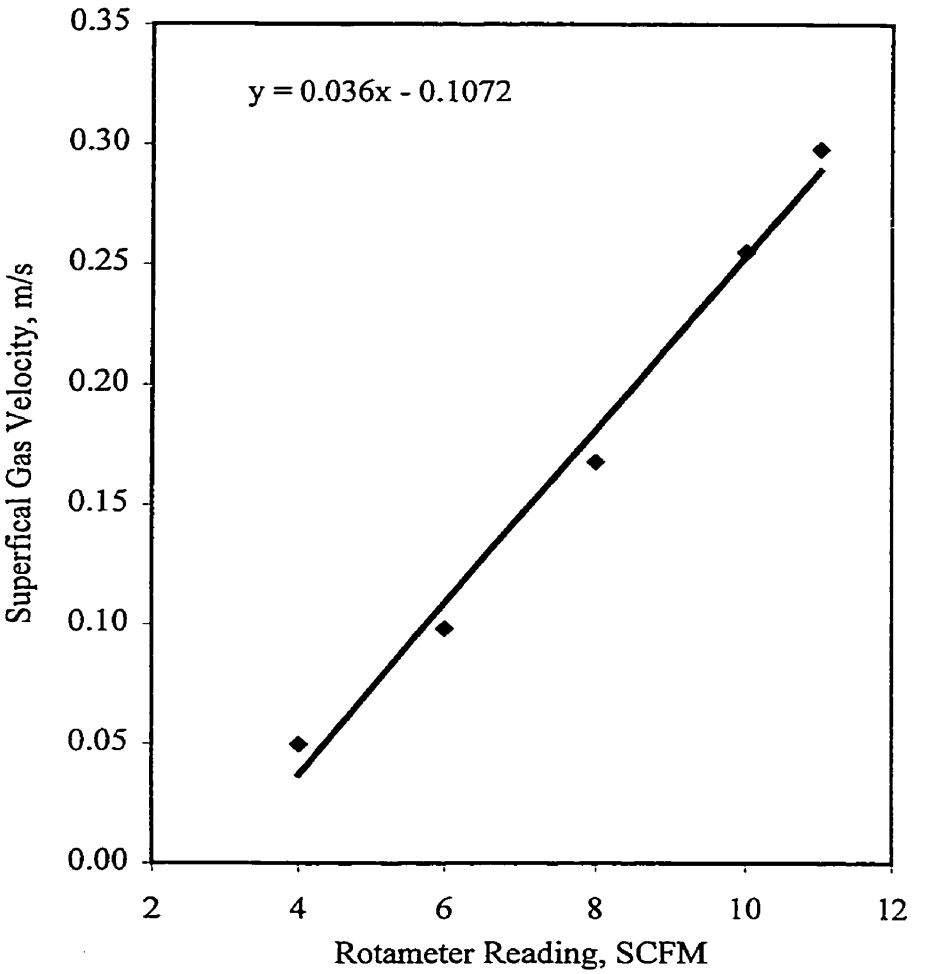

Figure A Rotameter Calibration Using Bell Prover

Appendix B

Needle Valve Calibration

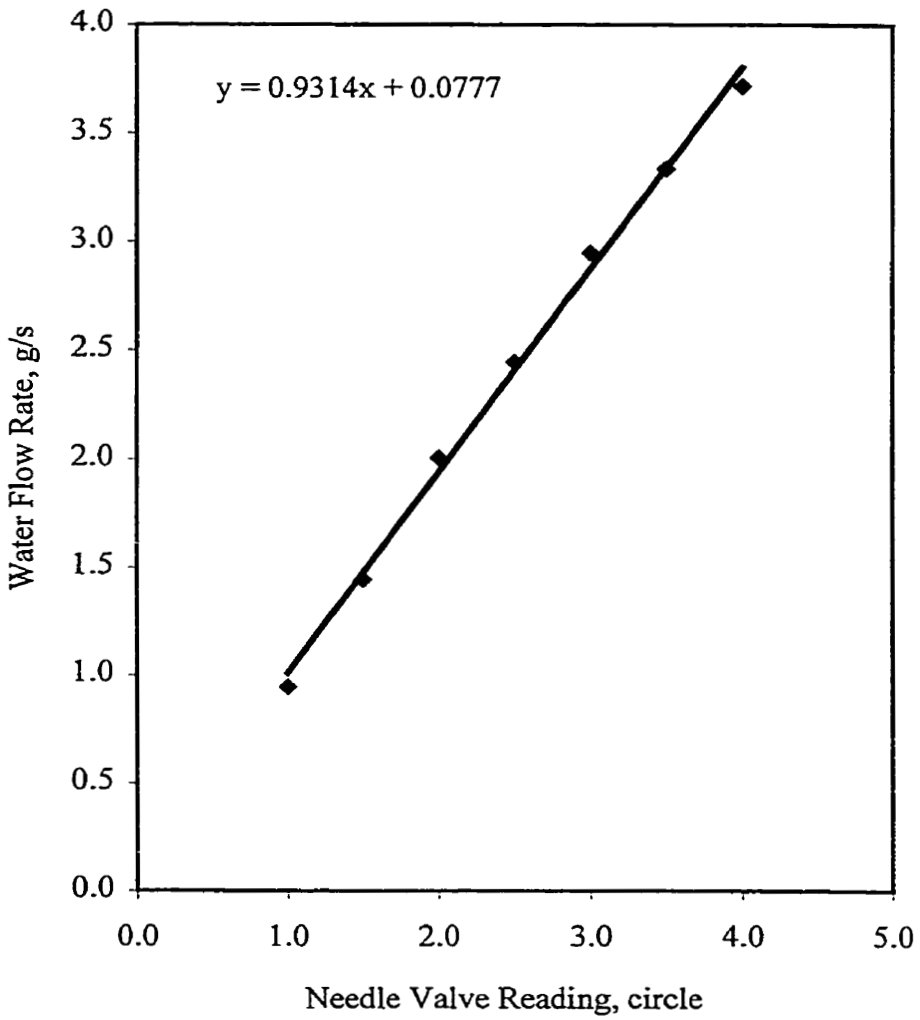

Figure B Needle Valve Calibration Using Stop Watch

Appendix C

Cumulative Mass Fraction Curve for Different Particles

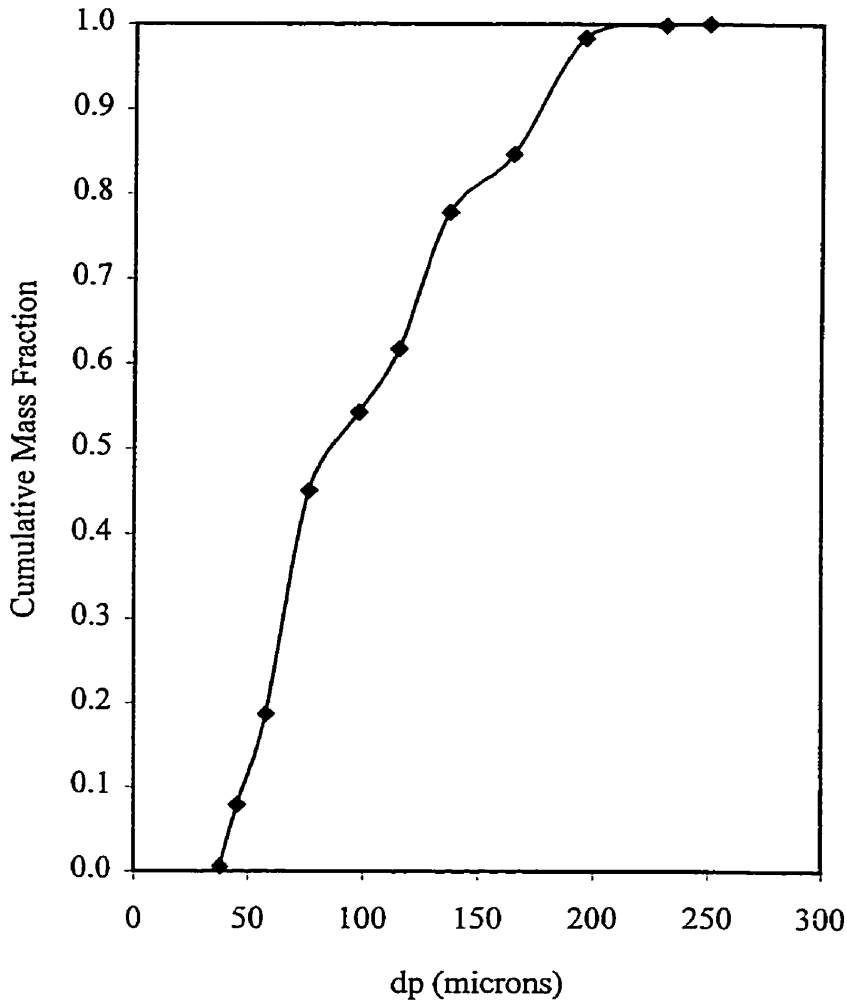

Figure C.1 Cumulative Mass Fraction Curve for FCC

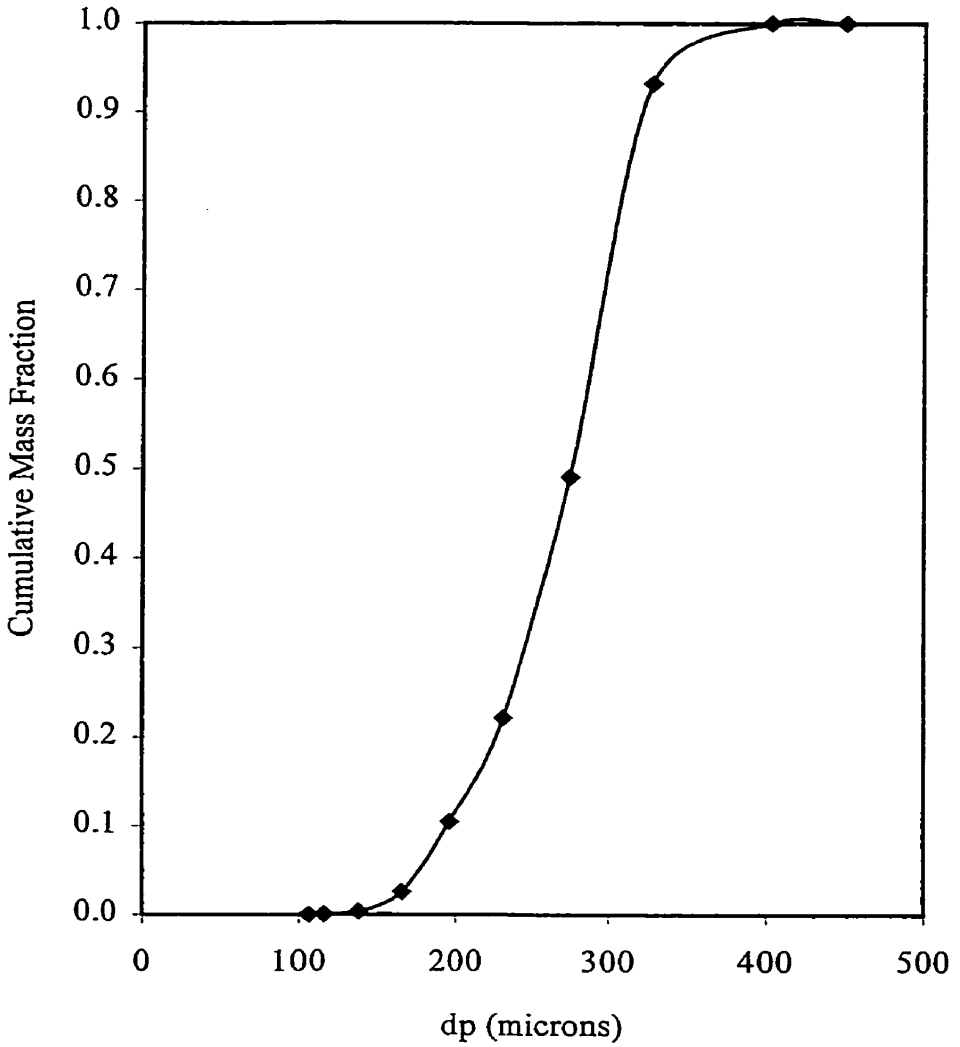

Figure C.2 Cumulative Mass Fraction Curve for Smaller Sand

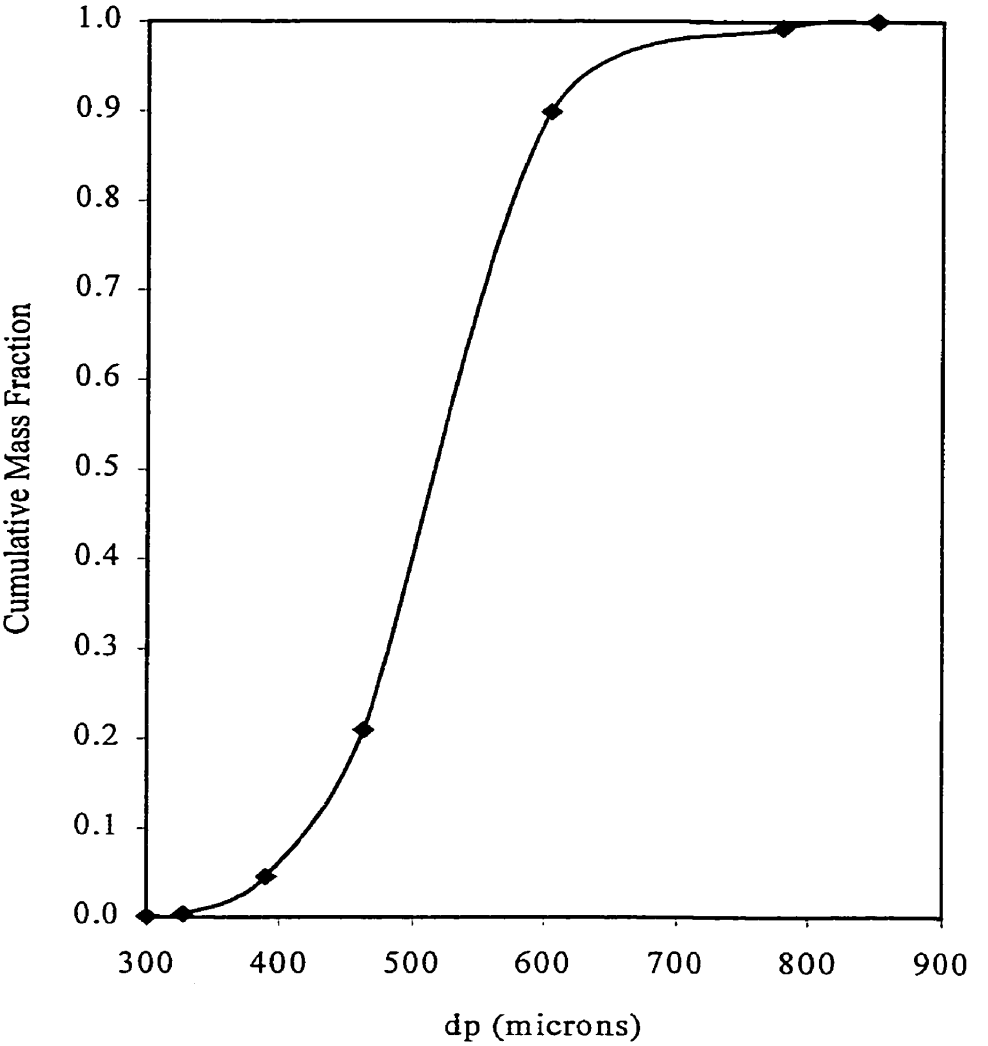

Figure C.3 Cumulative Mass Fraction Curve for Larger Sand

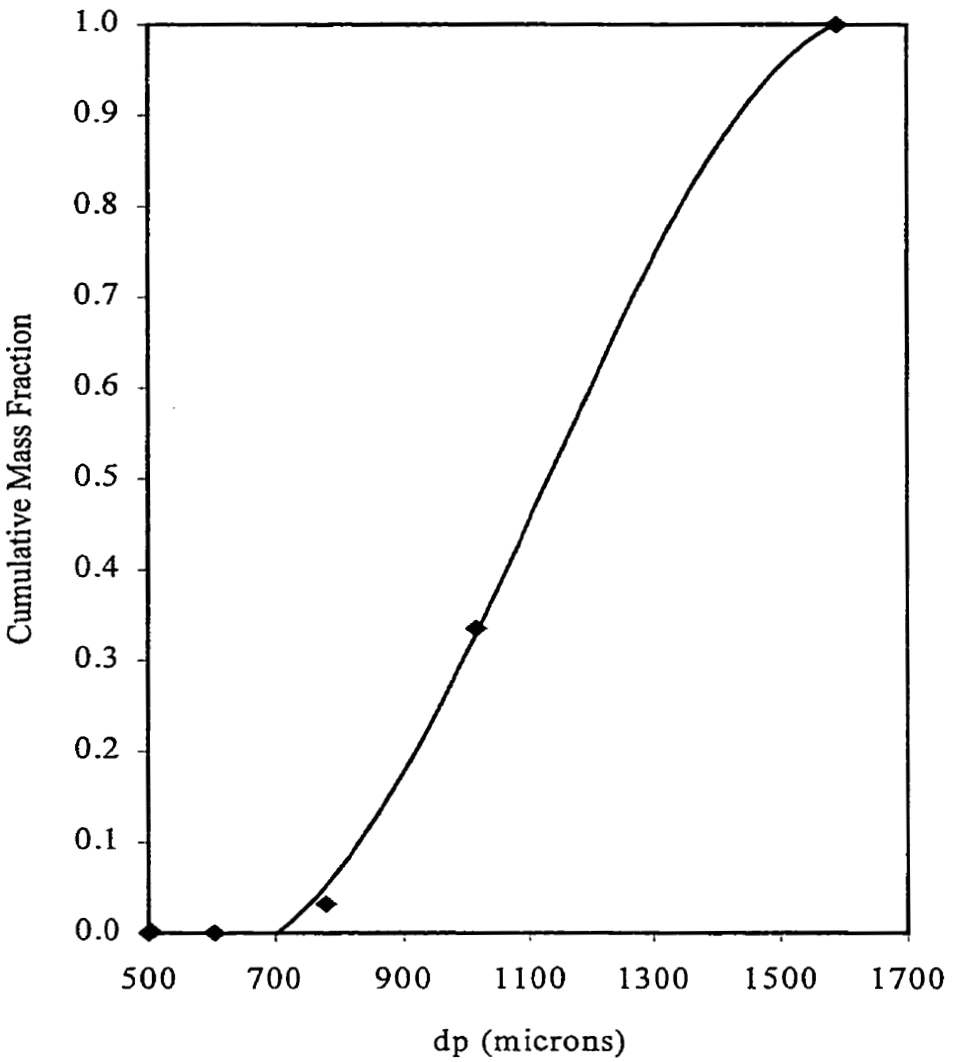

Figure C.4 Cumulative Mass Fraction Curve for Polystyrene